



## **Abstract**

Hydrogen is emerging as a promising energy carrier for storing renewable energy sources. Water electrolysis provides a clean and efficient production method, with alkaline water electrolysis being one of the technologies. However, a major limitation of this process is the low current density, which is partly caused by the formation of bubbles that affect the efficiency of the system. Understanding bubble dynamics and their impact on performance is important for optimizing hydrogen production. In this project, an attempt was made to predict the hydrogen bubble size distribution in the cathode - electrolyte interface using population balance modeling (PBM). Previous research focuses on using an experimentally determined bubble size distribution or a constant bubble size coming out from the surface of electrode, and using this as an input to the multiphase modeling of the electrolysis cell. Nucleation, growth, and detachment of hydrogen bubbles included in the model. The results are given in terms of the bubble size distribution and evolution of the mean diameters. The model results compared against experimental observations from literature. To check the applicability of the model the same approach was attempted to model the bubble size distribution of bubbles on a surface in a  $CO_2$  supersaturated solution. In this project, the applicability of population balance modeling to predict the bubble size distribution in alkaline water electrolysis is demonstrated and can be used as a starting point for future studies.

## **Acknowledgment**

This thesis report marks the culmination of my two-year Master's program in Hydrogen Systems and Enabling Technologies (HySET). I am extremely grateful to HySET for providing me with the scholarship opportunity and the chance to take part in this unique program.

I would like to express my sincere gratitude to my supervisors Prof. dr. ir. Martin van Sint Annaland and Dr. ir. I. Roghair, for their valuable guidance, support, and trust during this project. My heartfelt thanks go to my daily supervisor, Douwe Orij, whose encouragement, advice, and continuous support made this journey truly rewarding. My family. Lastly, I am thankful to my friends and colleagues, whose encouragement and companionship made this experience both inspiring and enjoyable.

## **Contents**

1	1.1 1.2 1.3	Alkaline Water Electrolysis	1 1 4 4
2	Poni	ulation Balance Modeling	5
_	2.1	Formulation of the Population Balance Equations	5
	2.2	Solutions to the Population Balance Equation	7
	2.2	2.2.1 Discretization	8
		2.2.2 Method of Moments	9
		2.2.3 Quadrature Based Method of Moments	9
		2.2.4 Choice of Solution Method	10
	2.3	Existing Works	11
	0	ZXISTING WORKS	
3	Bub	ble Evolution in Alkaline Water Electrolysis	19
	3.1	Bubble Nucleation	20
		3.1.1 Nucleating Experiments	24
	3.2	Bubble Growth	25
		3.2.1 Growth on the electrode surface	27
		3.2.2 Bubble growth in the bulk electrolyte	28
		3.2.3 Levels of Concentration	28
	3.3	Bubble Coalescence	30
	3.4	Detachment	30
	3.5	Additional Points regarding to the bubble behavior of Oxygen and Hydrogen	31
	3.6	Conclusion	31
4	D	Olation Delanas Madel Development	22
4	4.1	ulation Balance Model Development	<b>33</b>
	4.1	Model Description	34
		4.1.2 Solution to the PBM	35
	4.2	Population Balance Modeling of Bubbles in $CO_2$ Supersaturated Water Solution	36
	4.2	4.2.1 Constant Supersaturation $\dots$	36
		4.2.2 Variable Supersaturation	37
		T.2.2 Variable Supersaturation	31
5	Resu	ults and Discussion	39

#### Population Balance Modeling of Bubble Nucleation in Alkaline Water Electrolysis

	5.1	Hydrogen Bubble Size Distribution	39
		5.1.1 One - time Nucleation	39
		5.1.2 Continuous Nucleation	40
	5.2	Bubble Size distribution in $CO_2$ supersaturated solution	42
		5.2.1 Constant Supersaturation	42
		5.2.2 Variable Supersaturation	43
6	Con	nclusion and Outlook	45
-	6.1	Conclusion	45
	6.2	How can population balance modeling be used in discrete bubble modeling?	46
		· · ·	46
Α	Арр	pendix Title	53
	• •	Concentration as a function of current	53

viii

## **List of Figures**

1.1	Schematic representation of alkaline water electrolysis [7]	2
1.2	Individual contributions to the cell voltage [8]	3
1.3	Components of the cell resistance and their relative percentage [8]	3
2.1 2.2	Multiscale computational physics relevant to gas-evolving systems [10] Schematic of the curtain of width $\delta=2R$ , the volume gas fraction $\alpha$ , bubbles are represented by blue dots, and B) Notations used to write the Population balance	5
2.3	equations [24]	12 16
3.1	Schematic "life cycle" of a $H_2$ bubble during the hydrogen evolution reaction from an alkaline electrolyte [30]	19
3.2	Transport mechanism of dissolved gas from the electrode [48]	29
5.1	Comparison of bubble size distributions without and with diffusivity	40
5.2	Experimental bubble size distribution [51]	41
5.3 5.4	Comparison of mean diameters evolution without and with diffusivity	41
	cleation	42
5.5	Bubble size distribution in $CO_2$ bubbles	43
5.6	Bubble size distribution in $CO_2^-$ bubbles with variable supersaturation	43
A.1 A.2	Pathway of a general electrode reaction [57]	54
,	$x=0$ corresponds to the electrode surface, and $\delta_O$ is the diffusion layer thickness [57]	55

## Chapter 1

## Introduction

Nowadays, there is a growing use of fossil fuels together with the advancement of quality of life, industrialization of emerging countries, and the rise of the world's population. An increase in the speed of depleting fossil fuel reserves and substantial adverse effects on the atmosphere resulted from too much utilization of fossil fuels [1]. Renewable energies are energy sources that are continually replenished by nature and derived directly from the sun (such as thermal, photo-chemical, and photo-electric), indirectly from the sun (such as wind, hydropower, and photosynthetic energy stored in biomass), or from other natural movements and mechanisms of the environment (such as geothermal and tidal energy) [2]. Energy security concerns, struggles to alleviate the environmental impact of fossil fuels, and progress in a dominant role in encouraging renewable options have led to the radical increment in the utilization of renewable energy [3].

The intermittent nature of renewable energies makes it difficult to guarantee a steady supply of energy, even though they provide a sustainable and eco-friendly substitute for conventional energy sources. One potential solution is to convert renewable energy into chemical fuels that can be easily transported and stored, such as green hydrogen. Green hydrogen, which is generated by water electrolysis and renewable energy sources, has drawn interest as a potential energy carrier for industrial de-carbonization and as a way to store extra electricity [4]. With a simple method and hydrogen purity of greater than 99.9 %, water electrolysis is a type of clean and effective hydrogen production technology. However, this process only produces a small portion of the hydrogen produced worldwide. The high cost of electrolysis and the electricity consumption due to technological constraints are the causes. Current challenges in water electrolysis include reducing production and maintenance costs and energy usage while improving safety, durability, and reliability [5]. Alkaline water electrolysis (AWE), solid oxide water electrolysis (SOWE), and proton exchange membrane water electrolysis (PEMWE) are the three primary electrolysis technologies.

## 1.1 Alkaline Water Electrolysis

AWE has been mainly used for large-scale industrial applications for several decades. It is regarded a useful and economical way to produce hydrogen [4]. The cell is made up of two electrodes that are separated by diaphragm that is filled with an alkaline solution, usually 25 % - 30 % potassium hydroxide (KOH). Hydroxide anions( $OH^-$ ) are released when water splits at the cathode to produce

 $H_2$ , which then passes through the diaphragm and combines to make  $O_2$  at the anode [6].

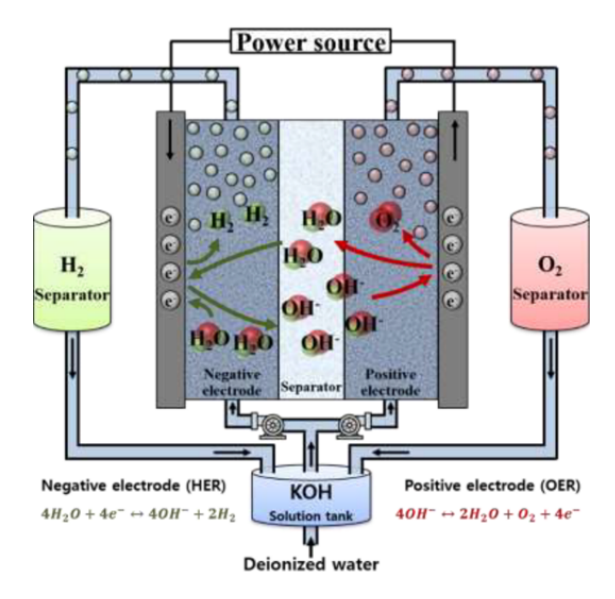


Figure 1.1: Schematic representation of alkaline water electrolysis [7]

The anodic and cathodic reactions of AWE are [8].

Anode:

$$4 \, \text{OH}^- \longrightarrow 2 \, \text{H}_2 \text{O} + \text{O}_2 + 4 \, \text{e}^- (E^0 = 0.40 V)$$

Cathode:

$$2 H_2 O + 2 e^- \longrightarrow H_2 + 2 OH^- (E^0 = -0.83V)$$

The actual cell voltage, which is the sum of the reversible potential, the overpotential of the anode and cathode electrodes, and the ohmic resistance, is given by:

$$E_{rev} = E_{anode} - E_{cathode} = 1.23V \tag{1.1}$$

$$E_{cell} = E_{rev} + \eta_{anode} + \eta_{cathode} + I \times R \tag{1.2}$$

$$R_{cell} = R_{circuit} + R_{electrolyte} + R_{bubbles} + R_{membrane}$$
(1.3)

AWE has a performance in the range of 59-70%, a working temperature of  $20-80^{\circ}\text{C}$  and a current density between 0.2 and 0.4  $A/cm^2$ . AWE has the advantage of lower capital costs compared to PEMW, and SOWE, and relatively stable and mature technology. However, a long starting time, a slow dynamic response, and a high corrosive due to the concentration of KOH electrolyte used are the drawbacks [5]. Improving the dynamic performance, and electrolysis efficiency are the current challenges in AWE.

One of the factors that affects the efficiency of AWE is the occurrence of bubbles. Bubbles can enhance mass transfer by promoting micro and macro-mixing. Bubble generation and detachment

can cause local agitation or micro-mixing of the electrolyte. Macro-mixing can also be caused by bubbles rising or migrating inside the bubble [9]. However, there are two major effects associated with it. Increased overpotential as the active surface area of the electrodes covered by the bubbles, and at higher current densities there are a lot more bubbles that give rise to an increased void fraction in the electrolyte which reduces the transport of OH ions [8]. The contributions of the actual cell voltage and the relative percentage of ohmic drop are illustrated in Figure 1.2 and Figure 1.3.

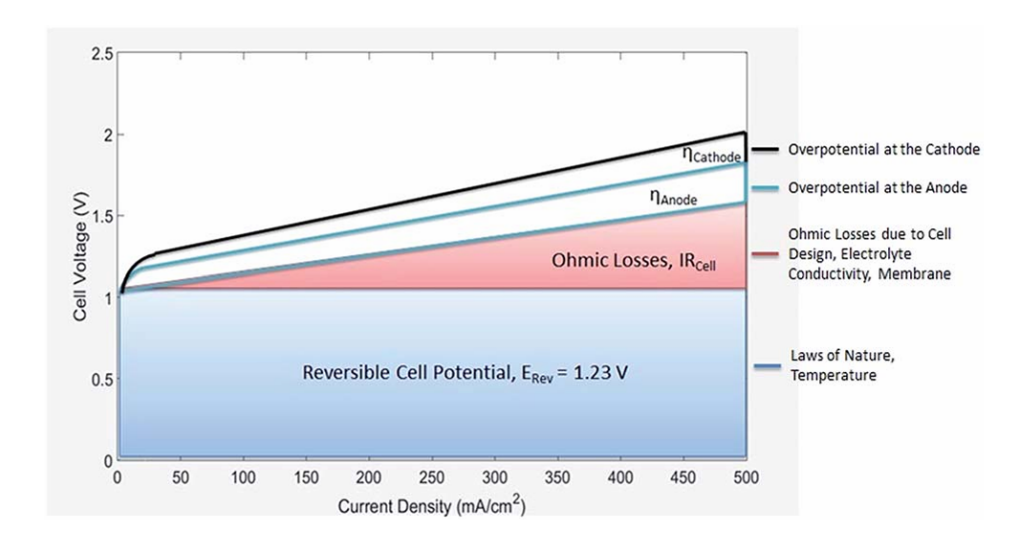


Figure 1.2: Individual contributions to the cell voltage [8].

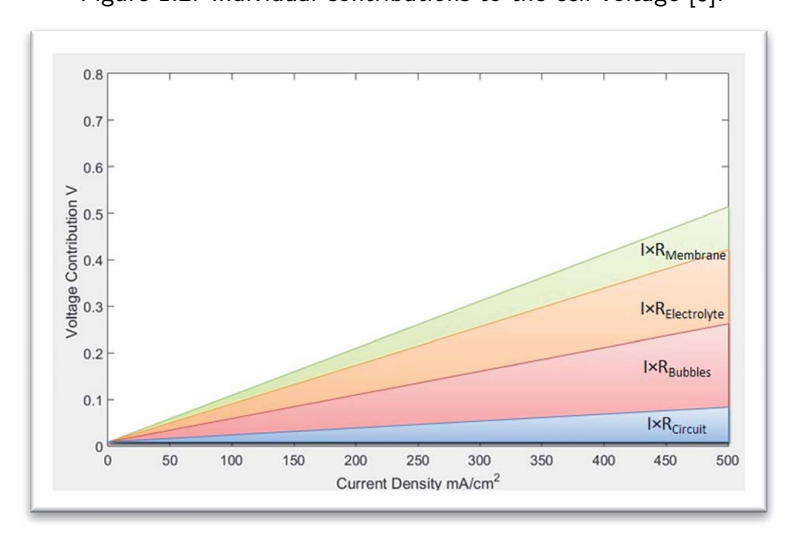


Figure 1.3: Components of the cell resistance and their relative percentage [8].

The presence of bubbles has the highest percentage in the ohmic losses and increases linearly with the current density. This study aims to better understand the bubble size distribution using population balance models. It is important to understand how bubbles behave in a system and affect performance.

#### 1.2 Research goals

The focus of this project is to investigate the nucleating bubble size distribution in the cathode - electrolyte interface in alkaline water electrolysis using population balance modeling (PBM). In order to achieve the aforementioned goal, the following specific objectives have been set.

- Literature review on Population Balance Modeling;
- Literature review on bubble nucleation in alkaline water electrolysis;
- Development of Population Balance Model;
- Perform simulations on bubble size distributions;
- Model Validation;

#### 1.3 Research Questions

The following research questions form the basis for this study. The first is given the most attention.

- How can population balance modeling be used to predict the bubble size distribution in alkaline water electrolysis?
- How can population balance modeling be used in discrete bubble modeling?

The format of this report is as follows. Chapter 2 discusses the nature of population balance modeling and previous studies on electrolytic bubble modeling. The bubble behavior in alkaline water electrolysis is explained in Chapter 3. Chapter 5 provides results and a discussion of the model development discussed in Chapter 4. The final chapter contains the conclusion and recommendations.

## Chapter 2

## **Population Balance Modeling**

Based on the characteristic lengths and temporal scales, the electrochemically gas - evolving system can be categorized into five computational groups. As illustrated in Figure 2.1, the computational models; quantum, molecular, mesoscale, continuum, and macroscopic; have temporal ranges between  $10^{-15}$  and  $10^0$  seconds and spatial scales between  $10^{-9}$  and  $10^0$ . Population balance modeling, are a class of computational techniques for mesoscale dynamics that effectively bridge the gap between continuum scales and molecular dynamics [10].

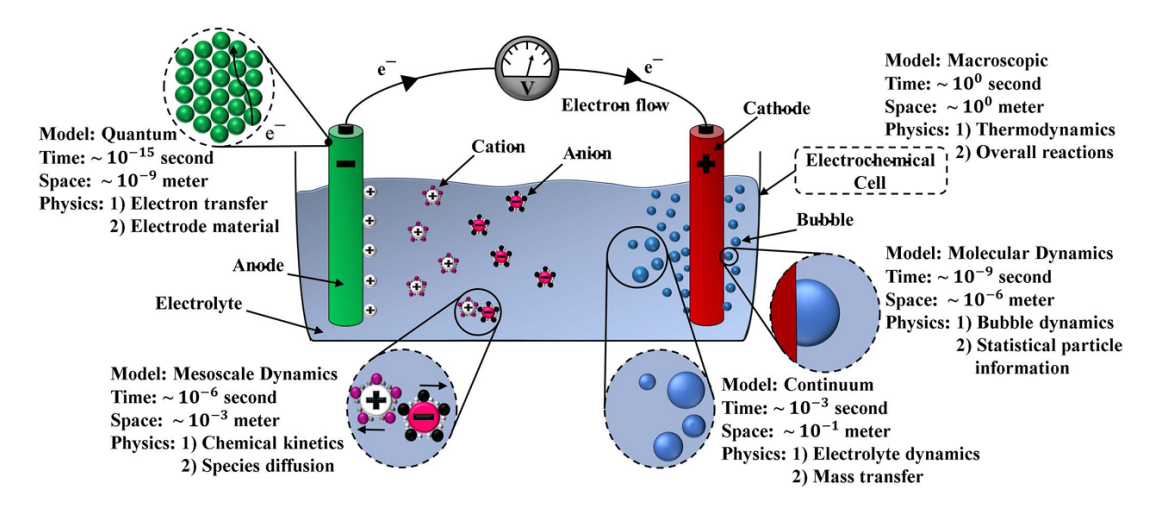


Figure 2.1: Multiscale computational physics relevant to gas-evolving systems [10]

## 2.1 Formulation of the Population Balance Equations

Dispersed-phase systems where particles are dispersed in a continuous phase are common in various processes, such as fluidized beds and crystallization. The particles have a considerable effect on the performance of such systems. The study of particulate systems aims to predict the properties of the population of particles and its surrounding from the characteristic of single particles in their local

environments. Appropriate extensive variables help to describe the population mainly the number of particles, mass, and volume of particles.

It is important to study the effect of the dispersed phase on the performance of the system. In order to understand this effect where the number of dispersed phases changes over time, population balances can be used [11]. Population balances have diverse applications in a wide range of dispersed phase systems, such as solid-liquid dispersions (with a particular emphasis on crystallization), and gas-liquid, gas-solid and liquid-liquid dispersions, microbial fermentors, polymer reactors [11], [12] [13].

The particles of interest, bubbles or crystals, are characterized by internal and external coordinates, called particle state. Internal coordinates, designated as  $\mathbf{x} \equiv (x_1, x_2, ..., x_d)$  are properties of the particle that describe its state such as size, chemical activity, chemical composition, and particle energy content. The location of particles in the physical space is the external coordinate, denoted as  $\mathbf{r} \equiv (r_1, r_2, r_3)$ . The particle state space is the combination of these two coordinates,  $\mathbf{R}(\mathbf{x}, \mathbf{r})[11]$ .

Every point in the particle state space has a particle number density is the basic assumption in the establishment of population balance equations [11]. The number density function, NDF, defines the distribution of the disperse phase elements over the properties of interest at any time instant and physical position. Given an arbitrary point in the phase-space  $(\mathbf{x}, \mathbf{r})$ , the NDF  $n(\mathbf{x}, \mathbf{r}, t)$  is defined as the expected number density of elements in the infinitesimal volume  $d\mathbf{x}d\mathbf{r}$  around that point at time t [14].

The average number density function represented by:

$$n(r;x,t) (2.1)$$

The population balance equation describes the evolution of the number density function and is given by [15]:

$$\frac{\partial}{\partial t} n(r;x,t) + \underbrace{\nabla_r \cdot [U_G n(r;x,t)]}_{\text{Convective in the physical space}} + \underbrace{\nabla_r \cdot [U_G n(r;x,t)]}_{\text{Convective in the physical space}} + \underbrace{\nabla_r \cdot [U_G n(r;x,t)]}_{\text{Convective in the physical space}} + \underbrace{\nabla_r \cdot [U_G n(r;x,t)]}_{\text{Convective in the physical space}} + \underbrace{\nabla_r \cdot [U_G n(r;x,t)]}_{\text{Convective in the physical space}} + \underbrace{\nabla_r \cdot [U_G n(r;x,t)]}_{\text{Convective in the physical space}} + \underbrace{\nabla_r \cdot [U_G n(r;x,t)]}_{\text{Convective in the physical space}} + \underbrace{\nabla_r \cdot [U_G n(r;x,t)]}_{\text{Convective in the physical space}} + \underbrace{\nabla_r \cdot [U_G n(r;x,t)]}_{\text{Convective in the physical space}} + \underbrace{\nabla_r \cdot [U_G n(r;x,t)]}_{\text{Convective in the physical space}} + \underbrace{\nabla_r \cdot [U_G n(r;x,t)]}_{\text{Convective in the physical space}} + \underbrace{\nabla_r \cdot [U_G n(r;x,t)]}_{\text{Convective in the physical space}} + \underbrace{\nabla_r \cdot [U_G n(r;x,t)]}_{\text{Convective in the physical space}} + \underbrace{\nabla_r \cdot [U_G n(r;x,t)]}_{\text{Convective in the physical space}} + \underbrace{\nabla_r \cdot [U_G n(r;x,t)]}_{\text{Convective in the physical space}} + \underbrace{\nabla_r \cdot [U_G n(r;x,t)]}_{\text{Convective in the physical space}} + \underbrace{\nabla_r \cdot [U_G n(r;x,t)]}_{\text{Convective in the physical space}} + \underbrace{\nabla_r \cdot [U_G n(r;x,t)]}_{\text{Convective in the physical space}} + \underbrace{\nabla_r \cdot [U_G n(r;x,t)]}_{\text{Convective in the physical space}} + \underbrace{\nabla_r \cdot [U_G n(r;x,t)]}_{\text{Convective in the physical space}} + \underbrace{\nabla_r \cdot [U_G n(r;x,t)]}_{\text{Convective in the physical space}} + \underbrace{\nabla_r \cdot [U_G n(r;x,t)]}_{\text{Convective in the physical space}} + \underbrace{\nabla_r \cdot [U_G n(r;x,t)]}_{\text{Convective in the physical space}} + \underbrace{\nabla_r \cdot [U_G n(r;x,t)]}_{\text{Convective in the physical space}} + \underbrace{\nabla_r \cdot [U_G n(r;x,t)]}_{\text{Convective in the physical space}} + \underbrace{\nabla_r \cdot [U_G n(r;x,t)]}_{\text{Convective in the physical space}} + \underbrace{\nabla_r \cdot [U_G n(r;x,t)]}_{\text{Convective in the physical space}} + \underbrace{\nabla_r \cdot [U_G n(r;x,t)]}_{\text{Convective in the physical space}} + \underbrace{\nabla_r \cdot [U_G n(r;x,t)]}_{\text{Convective in the physical space}} + \underbrace{\nabla_r \cdot [U_G n(r;x,t)]}_{\text{Convective in the physical space}} + \underbrace{\nabla_r \cdot [U_G n(r;x,t)]}_{\text{Convective in the physical space}} + \underbrace{\nabla_r \cdot [U_G n(r;x,t)]}_{\text{Convective i$$

Where  $U_G$  is the velocity of the dispersed phase assumed to be known,  $\Gamma$  the diffusivity, G(r) is the continuous rate of change in the space of internal coordinate, the growth rate of the

For a homogeneous and well mixed system, uniformly distributed in space, the spatial variation of particles can be neglected, and this assumption is considered in the subsequent discussions, and the number density function modified to:

$$n(x,t) (2.3)$$

The average number density function becomes mono variate when only one internal coordinate of the dispersed phase is taken into account; otherwise it is multi-variate. In this discussion, a mono variate number density function in terms of the size of bubbles is considered [16].

Open systems involve the transport of the dispersed phase along with the continuous phase that crosses the boundaries of the system, such as an electrolyzer with a flowing electrolyte. For such systems, the above equation without the diffusion term modified to:

$$\frac{\partial}{\partial t}(n(x,t)) + \frac{\partial}{\partial x}(G(x)n(x,t)) = \frac{V_{in}n_{in}(x,t) - V_{out}n(x,t)}{V_r} + h(x,t)$$
 (2.4)

Where  $V_{in}$  and  $V_{out}$  the inlet and outlet velocity respectively,  $V_r$  is the volume of the system.

The net source term, h(x,t) involves the birth and death of particles due to aggregation, A(x,t), and breakage, B(x,t), the birth of particles by nucleation, J(x,t). They are are represented in continuous coordinates as shown in the following equation [17],[13]:

$$A(x,t) = \frac{1}{2} \int_0^x n(x-x',t)n(x',t)Q(x-x',x') dx' - \int_0^\infty n(x,t)n(x',t)Q(x,x') dx'$$
 (2.5)

where Q(x, x') is the aggregation kernel.

The breakage function;

$$B(x,t) = \int_{x}^{\infty} \beta(x,x')\Gamma(x')n(x',t) dx' - \Gamma(x)n(x,t)$$
 (2.6)

and  $\beta(x, x')$  is the distribution of daughter particles, and  $\Gamma(x)$  is the breakage rate.

To fully describe the PBE equation above, the initial and boundary conditions needs to be specified. The initial condition:

$$n(x,t) = n_{\text{ini}}(x) = 0 \quad \text{for } t = 0, \ x > 0$$
 (2.7)

The boundary condition describes the number density at the smallest possible size of particles, and expressed by nucleation

$$G(0,t)n(0,t) = J(t)$$
 for  $t > 0, x \to 0$  (2.8)

The phenomenological processes involved in the population balance equations needs to specified for the system being considered. For this the nature of bubbles in alkaline water electrolysis and expression of the stages in the bubble evolution are discussed in Chapter 3.

#### 2.2 Solutions to the Population Balance Equation

Due to the nature of the equations, analytical solutions of integro-partial differential equations are difficult, and when they exist they are used as a comparison to numerical approaches. Fixed point methods such as method of successive approximations, and Laplace Transforms [11], and method of weighted residuals [18] can be used to give analytical solutions.

Discretization, method of moments, and quadrature based method of moments are the three main numerical approaches to the solution of population balance equations [14].

#### 2.2.1 Discretization

Discretization, or method of classes, is the based on dividing the internal coordinate space into a intervals (classes or sections) which transforms the PBE into a series of macroscopic balancing equations in the physical domain[14]. It takes a lot of computation to predict the number density n(x,t). As a result, the emphasis shifted from solving for the full number density to obtaining precise solutions for the quantities of interest such as the total number of particles and total mass (the first moment) [13].

The whole size range divided into small sections. The ith section is the size range that lies between two sizes  $x_i$  and  $x_{i+1}$ . The size  $v_i$ , the grid point, that represents the particle population in this size range, such that  $x_i < v_i < x_{i+1}$ .

Assuming the particle population is concentrated at representative sizes,  $v_i'$ s, the number density n(x,t) can be approximated to

$$n(x,t) = \sum_{k=1}^{M} N_k(t)\delta(x - v_k)$$
 (2.9)

For a PBE that involves nucleation, growth, and aggregation [19];

$$\frac{\partial n(x,t)}{\partial t} + \frac{\partial [G(x)n(x,t)]}{\partial v} = \frac{1}{2} \int_0^\infty n(x-x',t)n(x',t)Q(x-x',x') \, dx' - n(x,t) \int_0^\infty n(x',t)Q(x,x') \, dx' + S(x). \tag{2.10}$$

where G(x) is the growth rate for particles of size x, S(x) the rate of nucleation.

$$G(x) = \frac{dx}{dt} \tag{2.11}$$

The discretized form becomes

$$\frac{\mathrm{d}N_{i}(t)}{\mathrm{d}t} = \sum_{j,k}^{i \ge j \ge k} \left(1 - \frac{1}{2}\delta_{j,k}\right) \eta Q_{j,k} N_{j}(t) N_{k}(t)$$
for  $x_{i-1} \le (x_{j} + x_{k}) \le x_{i+1}$ 

$$-N_{i}(t) \sum_{k=1}^{M} Q_{i,k} N_{k}(t) + \int_{x(t)}^{x_{i}(t)+1(t)} S(x) \, dx$$

and

$$G(x_i) = \frac{dx_i}{dt} \tag{2.12}$$

where  $\eta$  evaluated as:

$$\eta = \begin{cases}
\frac{x_{i+1}(t) - v}{x_{i+1}(t) - x_i(t)}, & x_i(t) \le v \le x_{i+1}(t) \\
\frac{x_{i-1}(t) - v}{x_{i-1}(t) - x_i(t)}, & x_{i-1}(t) \le v \le x_i(t)
\end{cases} ,$$
(2.13)

where

$$N_i(t) = \int_{v_i}^{v_{i+1}} n(v, t) dv.$$
(5)

Different cases where pure growth, breakage and aggregation, as well as simultaneous breakage and aggregation, growth and aggregation, and nucleation and growth solved using this method [19],[13].

#### 2.2.2 Method of Moments

The method of moments tracks the evolution of moments of the number density distribution instead of the number density distribution [14], [15]. The moment method used to convert an intractable set of equations into a set of ordinary differential equations [20]. The  $j^{ih}$  moment of the number density normalized by the total number of particles defined as:

$$m_j = \int_0^\infty x^j n(x, t) \, \mathrm{d}x \tag{2.14}$$

The following quantities can be determined from the moments:

• The zeroth moment gives the total number of particles;

$$N_T = m_0 \tag{2.15}$$

• Sauter mean diameter,  $x_{32}$ , the most important particle size characteristics for many applications [16], and

$$x_{32} = \frac{m_3}{m_2} \tag{2.16}$$

• The volume averaged diameter,  $x_{43}$ , which can be equate as departure diameter of bubbles [21].

$$x_{43} = \frac{m_4}{m_3} \tag{2.17}$$

For lower order moments say from 0 to 5, expressing the higher order in terms of the lower one will not create a problem, however for higher order cases closure problem appears. Inability to express the higher order ones using the smaller ones. To correct this issue quadrature based of moments emerge as an alternative.

#### 2.2.3 Quadrature Based Method of Moments

The quadrature based method of moments is the development of the previous method of moments to avoid the closure issue. There are different variations of the quadrature methods [15].

Chapter 2. Population Balance Modeling

#### Quadrature method of moments

The unknown number density function ,NDF,is represented as a weighted summation of Dirac delta distributions  $\delta(x-x_{\alpha})$  in the QMOM approach:

$$n(x) \approx \sum_{\alpha=1}^{M} W_{\alpha} \delta(x - x_{\alpha})$$
 (2.18)

where  $W_i$  are non - negative weights of each kernel density function,  $x_i$  are the corresponding quadrature abscissa and N is the number of kernel density functions to approximate the NDF.

#### Direct quadrature method of moments

The direct solution of the transport equations for weights and abscissas of the quadrature approximation is the foundation of DQMOM. The weight and abscissa transport equations are expressed as follows:

$$\frac{\partial W_{\alpha}}{\partial t} + \nabla (\phi W_{\alpha}) = a_{\alpha} \tag{2.19}$$

$$\frac{\partial x_{\alpha}}{\partial t} + \nabla (\phi x_{\alpha}) = b_{\alpha}. \tag{2.20}$$

The solution of the following linear system in terms of the unknown  $a_i$  and  $b_i$  gives the value of  $a_i$  and  $b_i$ :

$$\sum_{\alpha=1}^{N} \left[ (1-k) x_{\alpha}^{k} a_{\alpha} + k x_{\alpha}^{k-1} b_{\alpha} \right] = \frac{1}{2} \sum_{\alpha=1}^{N} \sum_{\beta=1}^{N} W_{\alpha} W_{\beta} \left( x_{\alpha}^{3} + x_{\beta}^{3} \right)^{k/3} \beta(x_{\alpha}, x_{\beta}) - \sum_{\alpha=1}^{N} W_{\alpha} x_{\alpha}^{k} \sum_{\beta=1}^{N} W_{\beta} \beta(x_{\alpha}, x_{\beta}) + \sum_{\alpha=1}^{N} W_{\alpha} \bar{b}_{\alpha}^{(k)} a(x_{\alpha}) - \sum_{\alpha=1}^{N} W_{\alpha} x_{\alpha}^{k} a(x_{\alpha}), \qquad k = 0, 1, \dots, 2N - 1.$$
(2.21)

#### Extended quadrature method of moments

The unknown NDF approximated with a weighted sum of smooth, non-negative kernel density functions  $\delta_{\sigma}(x, x_{\alpha})$  in the EQMOM approach:

$$n(x) \approx p_N(x) = \sum_{\alpha=1}^{M} W_{\alpha} \delta_{\delta}(x - x_{\alpha})$$
 (2.22)

#### 2.2.4 Choice of Solution Method

The number of internal coordinates is a key factor while choosing the solution method. For univariate PBM, the method of classes (CM) and quadrature method of moments (QMOM) are suitable. If it is required to track the number density, CM works better. Conversely, some (usually measurable)

integral properties of the NDF can be obtained from QMOM. Interms of computing, the QMOM is typically less demanding than the CM. A considerable number of intervals or classes are typically required to achieve a reasonable accuracy by the CM, which is computationally intensive, especially when the dispersed phase cover a substantial section of the phase space. As a result, the QMOM is the recommended technique for the CFD simulation of spatially heterogeneous systems, particularly large-sale systems.

For systems comprised of continuous events - especially if the number of intervals cannot be expanded sufficiently - the CM should employ high-order techniques. However, using high-order methods typically results in instability. In contrast, if the growth rate is positive, QBMMs can readily handle continuous events. The value of the NDF at the origin of the pertinent internal coordinate can be estimated using the EQMOM in situations when growth rates are negative, such as evaporation or dissolution. Furthermore, when the particle processes of interest are strongly confined in the phase space, the EQMOM ought to be applied in most cases.

In addition, for highly localized phenomena, the CM or EQMOM are better suited in these situations. QBMMS are often recommneded techniques for bi- and multivariate PBEs [14]. In this work upwind finite difference method as described in the work of P.K. Inguva et al. (2022) [22] used.

#### 2.3 Existing Works

Existing research on the application of population balance modeling in electrolytic systems is covered in this section of the literature review. There are few studies on bubble dynamics of electrochemical systems, although population balance models have a wide range of uses in fields like pharmaceutical engineering, biotechnology and bioengineering, and energy fuels [23].

One comprehensive study is that of Bryson and Hofman (1989) [21] where the PBM was applied only to a particular system of the electrode surface. The equation was formulated as a conservation equation on the electrode's surface, relating the functional form of bubbles attached to it and the one departs from it.

$$accumulation = input - output + net\ generation$$
 (2.23)

Several assumptions were made, such that bubbles attached to the surface are spherical, that the system is sufficiently large to create steady state conditions, and that the effect of coalescence on the surface at lower current densities is negligible. Three density functions constituted the PBM.

- h(x)dx = fraction of bubbles nucleating on the electrode in the size range x to x + dx,
- f(x)dx = fraction of bubbles attached to the electrode in the size range x to x + dx,
- ullet g(x)dx= fraction of bubbles leaving the electrode in the size range x to x+dx

$$0 = qh(x) - qg(x) - \frac{d[Nu(x)f(x)]}{dx}$$
 (2.24)

Where N = total number of bubbles on the electrode per unit area; q = number of bubbles nucleating per unit area per unit time; u(x) growth rate of bubbles.

The distributions of f(x) and g(x) determined from the data obtained experimentally. A copper cathode, a lead anode, and a perspex glass make up the experimental setup. The bubbles sizes determined from images captured during electrolysis, and are fitted a log normal distribution.

The method of moments applied to solve the PBM, and two parameters are obtained. The growth coefficient  $\beta$ , and the departure diameter of the bubbles, and compared to the literature values.

In another work by Pierre Van de Velde et al. (2024) (preprint) [24] the PBM employed to investigate the impact of coalescence of bubbles at the apex of a horizontal electrode as shown in Figure 2.2.

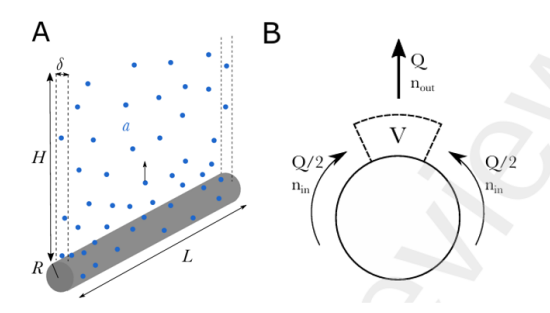


Figure 2.2: Schematic of the curtain of width  $\delta=2R$ , the volume gas fraction  $\alpha$ , bubbles are represented by blue dots, and B) Notations used to write the Population balance equations [24]

Assuming the bubbles path follows the shape of the wire, the PBE was set considering the incoming streams of bubbles of flow rate Q/2 from either side of the curtain and the exit stream of flow rate Q at the apex of the electrode of volume V.

$$\begin{split} V \frac{\partial n_{\mathsf{out}}(x,t)}{\partial t} &= Q \left( n_{\mathsf{in}}(x) - n_{\mathsf{out}}(x) \right) \\ &+ V \frac{1}{2} \int_0^x q(x,x-x') n_{\mathsf{out}}(x) n_{\mathsf{out}}(x-x') \, du \\ &- V \int_0^\infty q(x,x') n_{\mathsf{out}}(x') n_{\mathsf{out}}(x) \, dx' \end{split}$$

where q(x, x') is the aggregation rate.

By setting the inlet distribution  $n_{in}$  equal to the number distribution at the highest concentration of KOH where the effect of coalescence is minimum from experimental data the model is solved at steady state using the method of moments.

The effect of the coalescence explained by comparing the mean and variance of the distribution at different electrolyte concentration. At low coalescence efficiency, the mean volume of the input and output distributions are equal, while the variance increases slightly. However, at higher coalescence efficiency mean volume and variance of the output distribution increases significantly. The increase

in variance indicated that the wider distributions of the bubble size at higher coalescence efficiency.

The summary of these two papers in comparison with the general Population balance equation described below.

Aspect	General PBM Equation	Van de Velde et al. (2024)	Bryson and Hofman (1989)
Phenomena Mod- eled	General framework for particle size distribution evolution, including accumulation, growth, birth, death, and inflow/outflow.	Focuses on <b>coalescence</b> at the wire apex after bubble detachment. Growth and nucleation are not considered	Focuses on nucleation, growth, and detachment of bubbles attached to the electrode. Coalescence assumed to be negligible.
System Context	3D system (e.g., reactor) with volumetric number density $n(x,t)$ ( $m^{-4}$ ).	3D control volume at the wire apex, modeling bubble streams with volumetric number density $n(v,t)$ $(m^{-3}m^{-3})$ .	2D surface system (electrode) with surface number density $Nf(x)$ $(m^{-3})$ .
Characteristic Property	Size $x$ (general, e.g., diameter or volume).	Bubble volume $v$ , with $n(v,t)$ as the number density distribution.	Bubble diameter $x$ , with $Nf(x)$ as the number of attached bubbles per unit area.
PBM Equation	$\frac{\frac{\partial n}{\partial t} + \frac{\partial (Gn)}{\partial x}}{\overset{V}{\overset{(\text{in})}{n_i} - \overset{V}{\overset{(\text{out})}{n}}}} = B - D + \frac{1}{V}$	$\begin{array}{l} 0 = \frac{Q(n_{in} - n_{out})}{V} + \\ \frac{1}{2} \int_0^v q(u, v) - \\ u) n_{out}(u) n_{out}(v - u)  du - \\ \int_0^\infty q(u, v) n_{out}(u) n_{out}(v)  du \end{array}$	$0 = qh(x) - qg(x) - \frac{d}{dx}[Nu(x)f(x)]$
Accumulation Term	Rate of change of number density with time.	Set to 0 (steady state)	Set to 0 (steady state).
Growth Term	Change in number density due to growth, where $G$ is the growth rate $(ms^{-1})$ .	Not modeled, as bubbles are detached and growth is not considered in the control volume.	$\begin{array}{lll} \text{Modeled} & \text{as} \\ \frac{d}{dx}[Nu(x)f(x)], & \text{where} \\ u(x) & \text{is} & \text{the} & \text{growth} \\ \text{rate of diameter} & x, & \text{and} \\ Nf(x) \equiv n. \end{array}$
Birth Term (B)	Birth rate of particles (e.g., nucleation, aggregation) $(m^{-4}s^{-1})$ .	Bubbles of volume $\boldsymbol{v}$ formed by coalescence.	Nucleation: $qh(x)$ , rate of bubble nucleation per unit area $(m^{-2}s^{-1}m^{-1})$ .
Death Term (D)	Death rate of particles (e.g., breakage, detachment) $(m^{-4}s^{-1})$ .	Bubbles of volume $\boldsymbol{v}$ lost to coalescence.	Detachment: $qg(x)$ , rate of bubble detachment per unit area $(m^{-2}s^{-1}m^{-1})$ .
Inflow/Outflow Term	Convective transport of particles into/out of the system $(m^{-4}s^{-1})$ .	Modeled as $\frac{Q(n_{\rm in}-n_{\rm out})}{V}$ , where $Q$ is the volumetric flow rate of the bubble-liquid mixture $(m^3s^{-1})$ .	Not modeled $(=0)$ , as the system is a 2D surface with no convective flow into/out of a control volume.

Chapter 2. Population Balance Modeling

Key Assumptions	General form, can be transient or steady state, includes all possible processes.	<ul> <li>Steady state.</li> <li>Constant coalescence kernel q.</li> <li>No growth or nucleation in the control volume.</li> <li>Coalescence dominates.</li> </ul>	<ul> <li>Steady state.</li> <li>No coalescence (low current density).</li> <li>Growth follows diffusion-controlled model.</li> <li>Surface-based system.</li> </ul>
Current Density Range	Not specified (general).	High: 36 to 1785 $mA/cm^2$ , where coalescence is significant.	$ \begin{array}{llllllllllllllllllllllllllllllllllll$
Solution Method	Depends on the application (e.g., numerical, moments).	Method of moments to compute mean volume and variance of $n_{\rm out}(v)$ , focusing on coalescence effects.	Method of moments to relate moments of $g(x)$ (detaching) and $f(x)$ (attached), focusing on break-off diameter.
Input Distribution	$n_i$ , number density of incoming particles.	$n_{\rm in}(v)$ , approximated as $n_{\rm out}(v)$ at 2.5 M KOH (where coalescence is minimal).	h(x), nucleation distribution, assumed negligible for higher moments (small nucleation sizes).
Results	Depending on the application.	Mean volume and variance of the input and output distributions calculated, and the values increased after coalescence.	The bubble break off diameter, $x_{43}$ , and growth coefficient $\beta$ calculated.

Table 2.1: Comparison of the general PBM equation with the PBMs in Van de Velde et al. (2024) and Bryson and Hofman (1989).

The comparison indicates that the choice of the system determines the modeling approach used. The number distribution in both cases was not tracked down, the simulation results expressed in terms other quantities that are characteristic of the population. Despite the nucleation of bubbles included in the work of Bryson and Hofman (1989) [21], the rate was not calculated separately and included in the population balance equation.

Computational fluid dynamics (CFD) and population balance modeling (PBM) have been used in previous studies to predict two-phase flows in electrolysis cells. PBM is used in these models to monitor the bubble size distribution, while the CFD is in charge of capturing the system's hydrodynamics.

In the study by Zhan et al. (2017) [25], for example, three-dimensional numerical simulations of gas-liquid two-phase flow were conducted for a three-anode and scaled-up 300 kA aluminum electrolysis cell. These simulations integrate PBM and CFD, treating the dispersed phase (anode gas) and continuous phase (electrolyte) as interpenetrating phenomena using the Euler-Euler two-fluid model.

In contrast to traditional Euler-Euler models, which assume a constant mean bubble diameter, Zhan

et al.'s approach utilizes PBM to represent the dynamic evolution of bubble size distribution. The PBM takes into consideration the birth and death of bubbles as a result of coalescence and breakage processes in the electrolyte region. The PBM is given by:

$$\Delta \cdot (\mathbf{u}_g n_i) = B_B - D_B + B_C - D_C \tag{2.25}$$

where  $n_i$  is the number density function of group i bubbles.

The solution of the PBEs is carried out using the method of classes (CM), where different bubble size gruops are tracked and implemented in the current CFD approach. Then, the steady-state PBEs for the ith bubble class can be expressed as

$$\nabla \cdot (\alpha_q \rho_q \mathbf{u}_q f_i) = B_{\mathsf{Bi}} - D_{\mathsf{Bi}} + B_{\mathsf{Ci}} - D_{\mathsf{Ci}}$$
(2.26)

Here,  $f_i = \alpha_i/\alpha_g$  represents the volume fraction of bubble group i, with the constraint that the sum of all class volume fractions equals the local gas volume fraction  $\alpha_g$ . The relationship between  $f_i$  and the number density  $n_i$  is given by:

$$\alpha_g f_i = n_i V_i \tag{2.27}$$

The initial bubble size at the inlet was set to 1mm with a volume fraction of 1.0. The PBM-CFD coupling is achieved through the calculation of the Sauter mean diameter,  $d_{32}$ , evaluated as:

$$d_{32} = \frac{\sum_{i=1}^{N} n_i d_i^3}{\sum_{i=1}^{N} n_i d_i^2} \qquad i = 1, 2, ..., N$$
 (2.28)

This diameter is essential for creating calculating interphase forces and bubble-induced turbulence (BIT), thereby establishing a feedback loop between the PBM and CFD models. PBM provides detailed bubble size information, while CFD supplies the necessary two-phase flow field [25]

In another study, Nierhaus et al. (2009) [26] performed two-phase flow simulations in an electrolysis cell with an inverted rotating disk electrode (IRDE). The bubble motion was tracked using an Eulerian-Lagrangian model. The work involves optical imaging of the bubbles at the top and rear side of the electrode. The bubble size distributions determined at the top of the electrode, and fitted to a log normal distribution.

This experimental data was later used in the CFD-PBM single fluid modeling of water electrolysis by Askari et al. (2018) [15]. The moments of distribution were applied as an ingoing boundary condition for the single fluid CFD-PBM coupling.

The PBM focuses on the bubble coalescence and breakage processes, and were solved using the Extended Quadrature Method of Moments (EQMOM) and the bubble size distribution at the boundary were reconstructed. However, these models focus on the bubble behaviour in the bulk electrolyte and generally exclude electrochemical phenomena occurring at the electrode- electrolyte interface.

The focus of the present work is to address this gap by modeling the population balance of nucleating bubbles on the surface of the electrode. Unlike bulk bubble distributions, which typically range

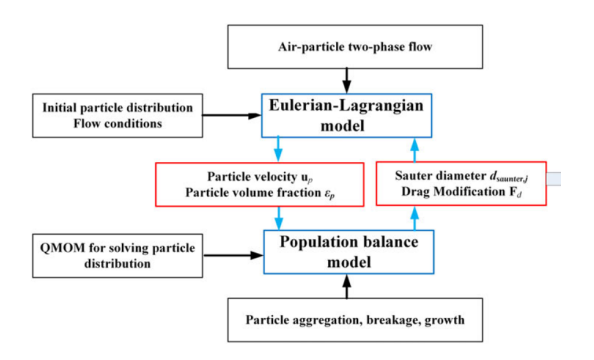


Figure 2.3: Coupling of Euler -Lagrangian Simulation with Population Balance Modeling [27]

in the millimeter scale, nucleating bubbles involve microscopic scales and require distinct modeling approaches.

Population balance modeling can be coupled with Euler - Lagrangian simulation as shown in Figure 2.3. Discrete bubble modeling (DBM) applied to investigate the mechanism of bubble nucleation in a  $CO_2$  supersaturated solution according to the work of Battistella et al. (2021) [28]. The following comparison between these approaches is drawn in relation to modeling the the bubble dynamics.

Table 2.2: Comparison between Population Balance Modeling (PBM) and Discrete Bubble Modeling (DBM)

Aspect	Population Balance Modeling (PBM)	Discrete Bubble Modeling (DBM)
Nucleation	Based on statistical nucleation theories and empirical correla- tions, less attention to site spe- cific behaviour	Modeled using predefined nucleation sites and local supersaturation conditions govern bubble formation
Growth and Mass Transfer	Captures averaged growth across the bubble population. The gas-phase sink tern is calculated by integrating over the population.	Resolves the growth dynamics of individual bubbles. Mass transfer rates are computed per bubble and summed to obrain the total sink term
Detachment Criteria	Averaged departure behavior; bubbles depart when they reach a prescribed departure size	Each bubble detaches when it individually exceeds its departure size, Frtiz correlation
Coalescence and Breakage	Modeled statistically using kernels and statistical operators within the population balance equation	Explicitly resolved as physical overlap or proximity events between individual bubbles
Computational Cost	Relatively low; efficient for sim- ulating large systems with many bubbles. Suitable for obtaining average behavior and statistical trends	High; computationally expensive due to tracking individual bubbles in time and space
Spatial Resolution	Spatially averaged; bubble interactions are resolved in number or size space, not physical space	High spatial resolution; bubble locations and interactions are resolved in physical 3D space

## Chapter 3

# Bubble Evolution in Alkaline Water Electrolysis

Alkaline water electrolysis constitutes a two-phase dispersed system, with the dispersed phase comprising the bubbles [29]. A finite volume of gas enclosed within one or more continuous solid or liquid phases is called a bubble. Free bubbles, which are contained within a single phase in the bulk electrolyte, and interfacial bubbles, that are present at the interface of two bulk phases, such as the electrode/electrolyte interface, are the two subcategories that can be differentiated based on the organization of the gas interfaces [30]. Bubbles detach from the surface and enter in to the bulk electrolyte during detachment 3.1.

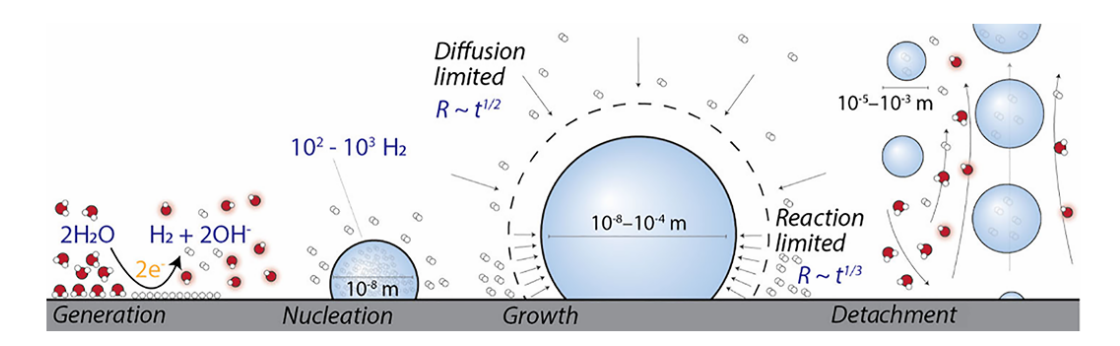


Figure 3.1: Schematic "life cycle" of a  $H_2$  bubble during the hydrogen evolution reaction from an alkaline electrolyte [30]

The four stages of a bubble's life cycle at a gas-evolving electrode are usually nucleation, growth, coalescence, and detachment. The random creation of a cluster of gas molecules from a solution supersaturated with dissolved gas is known as nucleation. Following nucleation, the bubble keeps expanding by absorbing more molecules of the dissolved gas. The buoyant force acting on the bubble increases with its size. The bubble is raised and subsequently separates from the electrode surface when the buoyant force is sufficient to overcome the adhesion force holding it there. When two bubbles come into contact, either in the solution or on the electrode, coalescence takes place, lowering the

total surface energy [31].

#### 3.1 Bubble Nucleation

Nucleation is the generation of particles, bubbles, from molecules dissolved in the continuous phase, and it is the first step in the evolution of bubbles [30]. Nucleation involves the process of formation of a new thermodynamic phase from an old phase with free energy to an organized structure or pattern with low free energy [32]. The nucleation process is described by classical nucleation theory, and its rate is written as:

$$J = J_0 \exp\left(\frac{-16\pi\gamma^3\phi(\theta)}{3k_BT \left(P_{gas} - P_0\right)^2}\right)$$
 (3.1)

The pre-exponential factor,  $J_0$ , describes the statistical molecule-by-molecule process of nucleus growth [33], and  $\phi(\theta)$  is the geometric factor which represents the reduction in the surface energy due to the presence of solid surface.

$$\phi(\theta) = \frac{(2 - \cos \theta)(1 + \cos \theta)^2}{4} \tag{3.2}$$

 $P_{gas}$  denotes the partial pressure of gas inside the bubble and  $P_0$  is the ambient pressure. The partial pressure of gas in the bubble,  $P_{gas}$ , is approximately equal to the gas pressure in the bubble,  $P_{bubble}$ , which can be expressed by the Laplace Pressure. Since gas evolving electrodes typically produce purified gases, the two pressure values can be taken as equal [30]:

$$P_{bubble} = P_0 + \frac{2\gamma}{r} \tag{3.3}$$

The ratio of  $P_{bubble}$  to  $P_0$  is the supersaturation that drives nucleation. It can also be given as is the ratio of the dissolved gas concentration at the electrode surface,  $C_{surf}$  to the concentration in the bulk ,  $C_{\infty}$ . Generally, for nucleation to occur,  $\zeta$  must be greater than 100. [10].

In another study by Lee J. et al. (2022) [34], where the gas evolution processes are modeled on porous electrodes of zero-gap alkaline water electrolysis cells, the critical gas concentration is given as:

$$C_{bn,i} = \frac{2\gamma H_i}{e} \frac{1}{r_{tm}} \tag{3.4}$$

Where  $C_{bn,i}$ , is the critical gas concentration at which bubble nucleates,  $r_{bn}$  is the nucleation bubble radius, and e is the Euler number.  $H_i$  is the Henry's constant which is given by

$$H_i = H_i^0 \exp\left[-\frac{\Delta H}{R} \left(\frac{1}{T} - \frac{1}{298K}\right)\right]$$
 (3.5)

where  $H_i^0$  is Henry's coefficient at 298~K and  $\Delta H$  is the enthalpy of dissolution [34].

The above concentration can be translated to pressure using Henry's law and used to calculate the nucleation rate according to Equation 3.1 as a function of the working temperature of an electrolysis cell

However, for electrochemical cells it is important to relate the nucleation rate with parameters such as current density and overpotential values. In this regard, the Gibbs free energy of nucleation formation and the critical radius are written as: as [10], [35]:

$$\Delta G_{\text{het}}^{\ddagger} = \phi(\theta) \frac{16\pi \gamma^3 V^2}{3(zF\eta)^2} \tag{3.6}$$

$$R_c = \frac{2\gamma V}{zF\eta} \tag{3.7}$$

The rate equation can be given as:

$$J = DCexp\left(-\frac{\Delta G_{Het}^*}{k_B T}\right) \tag{3.8}$$

$$J = DCexp\left(-\frac{16\pi\gamma^3 V^2 \phi(\theta)}{3k_B T (zF\eta)^2}\right)$$
(3.9)

where  $D \mod m^{-3} \ s^{-1}$  denotes the flow of molecules that are added to the forming nuclei;  $C \pmod{mol^{-1}}$  the concentration of molecules (nuclei consisting of a number of molecules);  $V \pmod{mol^{-1}}$  the specific volume of the nucleating bubble; z is the number of charges transferred;  $\eta(V)$  the electrode overpotential.

#### Overpotential

Once the overpotential of the electrode is known, the nucleation rate can be calculated according to Equation 3.9. Recall that the actual cell voltage for alkaline water electrolysis is composed of the overpotential of the anode, cathode, and ohmic resistance.

$$E_{cell} = E_{rev} + \eta_{anode} + \eta_{cathode} + I \times R \tag{3.10}$$

Evaluating the rate of nucleation for hydrogen and oxygen bubbles requires determining the cathode and anode overpotential, respectively. It can be determined experimentally through the electrochemical characterization of the alkaline electrolysis cells. According to the work of Thijs de Groot et al. (2024) [36] electrochemical impedance spectroscopy (EIS) and polarization curves yield important information about the overpotential. A combined overpotential value of  $\eta_a + \eta_c$  in the range 0.6-1.0V depending on the current density for a two-electrode flow cell configuration determined at room temperature and atmospheric pressure.

One remark about the usage of equation 3.9 is that term inside the exponent becomes extremely negative at room temperature and atmospheric pressure and results in zero value. Random calculation of the nucleation rate at  $\eta_c = 0.4~V$  at room temperature and atmospheric pressure gives a value of zero. To avoid this, a relatively higher temperature and pressure is required, for example, at  $60^{\circ}C$ 

and  $30\ atm$ . These values result is a smaller molar volume value in the range of  $10^{-4}\ m^{-3}/mol$ , its squared in the numerator of the exponential term compensated by the very small value from the denominator. However, bubble nucleation is observed at room temperature and atmospheric pressure, and this equation is not applicable at these conditions.

Besides electrochemical characterization, empirical equations can be used to relate the overpotential with other parameters. These relations can be found in the work of Daoudi C and Bounahmidi T (2024), in which an overview of alkaline water electrolysis modeling is discussed [4].

#### Overpotential:

$$\eta_c = \frac{RT}{\alpha_c F} \ln \left( \frac{i}{i_{0,c} (1 - \varnothing)} \right) \tag{3.11}$$

$$\eta_a = \frac{RT}{\alpha_a F} \ln \left( \frac{i}{i_{0,a} (1 - \varnothing)} \right) \tag{3.12}$$

Bubble coverage rate: [4] & [37]

$$\varnothing = 0.023(i)^{0.3} \left(\frac{T}{T_{\text{ref}}} \frac{P_{\text{ref}}}{P}\right)^{1.5}$$
 (3.13)

Exchange current density: [4] & [38]

$$i_{0,a} = 0.9 \times 10^{-4} \left(\frac{P}{P_{\text{ref}}}\right)^{0.1} \exp\left[\frac{-42000}{RT} \left(1 - \frac{T}{T_{\text{ref}}}\right)\right]$$
 (3.14)

$$i_{0,c} = 1.5 \times 10^{-4} \left(\frac{P}{P_{\text{ref}}}\right)^{0.1} \exp\left[\frac{-23000}{RT} \left(1 - \frac{T}{T_{\text{ref}}}\right)\right]$$
 (3.15)

#### Charge transfer coefficient:

$$\alpha_c = 0.1175 + 0.00095T \tag{3.16}$$

$$\alpha_a = 0.0675 + 0.00095T \tag{3.17}$$

where i, the current density,  $T_{\mathsf{ref}}$  and  $P_{\mathsf{ref}}$  the reference temperature and pressure.

These correlations can help to determine the overpotential at various current density values.

Alternatively, the number of bubbles generated during the electro-flotation of water can be calculated by the following formula according to the work of R.R. Hacha et al. (2019) [39].

$$N = \frac{\Phi Q_g}{\pi d_s^3 / 6} \tag{3.18}$$

Where N is the number of bubbles produced;  $\Phi$  is the sphericity of bubbles,  $Q_g$  the gas generation rate, and  $d_b$  is the Sauter bubble diameter.

Images captured during the experiment and the diameter of bubbles analyzed by a bubble sizer, the Sauter bubble diameter calculated from individual bubble diameter values as

$$d_{32} = \sum_{i=1} d_i^3 / \sum_{i=1} d_i^2 \tag{3.19}$$

where  $d_i$  is the bubble diameter.

The gas generation rate  $Q_q(L/s)$  is given by:

$$Q_g = \frac{IV_o}{nF} \tag{3.20}$$

where I is the current intensity (A);  $V_0$  is the molar volume  $(22.4 \ L/mol)$ ; n is the number of electrons; and F is the Faraday constant.

However, this analysis made the assumption that all of the gas produced helps create bubbles, which is untrue in electrolysis cells.

#### The Pre-exponential Factor

The term under the exponent is usually very small and the numerical value of the nucleation rate mainly depends on the pre-exponential factor,  $J_0$ . It's value is with in the range of  $10^{20}m^{-2}s^{-1}$  for heterogeneous classical nucleation [40].

Following the description of D and C in Equation 3.9, The value of D is the amount of produced gas at the electrode and partially remained attached to the electrode surface, designated by  $N_G$ . The discussion of this topic is found in section 3.2.3. Assuming that all of this amount contribute to the formation of bubbles

$$D = f_G \frac{i}{zF} \left( mol/m^2 S \right) \tag{3.21}$$

where  $f_G$  is the fraction of produced gas accumulated on the electrode surface.

The value of  $C\ nuclei/mol$  can be estimated as the number of nuclei per a single mole of the dissolved gas.

$$C = \frac{N_A}{N_{cr}} \tag{3.22}$$

23

where  $N_A$  is Avogadro's number,  $N_{cr}$  is the number of atoms at the critical size of nuclei which is related to the critical radius and overpotential and given by [41]:

$$N_{\text{critical}} = \frac{16\pi N_A V^2 \gamma^3}{3(zF\eta)^3} \tag{3.23}$$

Chapter 3. Bubble Evolution in Alkaline Water Electrolysis

The product of these terms would give the pre-exponential factor.

$$DC = f_G \frac{i}{zF} \times \frac{3(zF\eta)^3}{16\pi V^2 \gamma^3} \frac{nuclei}{m^2 s}$$
(3.24)

#### 3.1.1 Nucleating Experiments

Measuring the supersaturation is necessary to predict the nucleation rate in accordance with the Classical Nucleation theory, CNT. It can be measured experimentally using two methods: counting the number of bubbles for water supersaturation by  $CO_2$  [42], and measuring the induction time for electrode nucleation. The latter is discussed here.

Induction time which denotes the time required to attain the necessary supersaturation of the electrolyte with respect to dissolved gas at the electrode surface measurement applied for the nucleation of hydrogen [40] and oxygen bubbles in the work of [33].

In these two experiments the induction time measured as a function of applied current. The value of the applied current,  $i_{app}$  set below a maximum value which is the peak current  $i_{nb}^p$  where the nucleation of bubbles becomes non spontaneous. The electrodes used were disk shaped ultra micro electrodes.

Using Henry's law the  $P_{gas}$  can be expressed in terms of the surface concentration as

$$P_{gas} = C_{surf} K_H \tag{3.25}$$

The surface concentration can be written as a function of the applied current as

$$C_{H_2}^{surf} = \frac{i}{4nFD_{H_2}a} {3.26}$$

where a is the apparent radius of the electrode. The derivation of these equations is presented in the Appendix.

The rate of nucleation can be given as a function of current as:

$$J = J_0 \exp\left(\frac{-16\pi\gamma^3\phi(\theta)}{3k_B T \left(\frac{i}{K_H 4n FaD_{H_2}} - P_{\text{ambient}}\right)^2}\right)$$
(3.27)

In the work of German et al [40] the nucleation rate determined as:

ullet The cumulative probabilities; P(t) the probability that a bubble has nucleated by time t of calculated by

$$P = \frac{N^+(t)}{N} \tag{3.28}$$

Where N is the total number of measurements at each current and  $N^+(t)$  is the total number of measurements in which a bubble has formed by time t.

• The experimental data fit to a distribution

$$P(t) = 1 - exp(-J(t - t_{limit}))$$
(3.29)

and J determined as a model fit.

• The value of contact angle  $\theta$ , and pre exponential factor  $J_o$  determined from a plot of

$$\ln J vs \frac{1}{\left(\frac{i}{K_H 4nFD_{H_2}a} - P_0\right)^2}$$

and the activation energy as

$$E_a = \frac{-kT * Slope}{\left(\frac{i}{K_H 4nFD_{H_2} a} - P_0\right)^2}$$

In the oxygen nanobubbles [33]:

• The rate of nucleation estimated from

$$J \approx 1/(\bar{t_{ind}} - t_{limit})$$

where  $t_{ind}^-$  is the mean value of the nucleation time at a certain  $i_{app}$ , and  $t_{limit}$  is the shortest accessible time.

ullet The value of the  $J_0$  and B determined as a best fit parameter from the plot of

$$ln\left(\frac{J_0}{J}\right) = B \frac{1}{\left(\frac{i}{K_H 4nFD_{O_2}a} - P_0\right)^2}$$

where 
$$B = 16\pi\gamma^3\phi(\theta)/3kT$$

The comparison of the two papers is given in Table 3.1.

The induction time measurements, the CNT predicts the rate for

- Ultra micro electrodes (UME) that exhibit steady state behavior;
- Single nanobubbles originating from a known nucleating sites

However, for conventional electrodes with numerous nucleation sites, larger surface area, and all mass transfer mechanisms (diffusion, migration, and convection) are involved the rate prediction could be challenging. The bubbles are directly related to the amount of current applied which determines the rate of generation of the hydrogen or oxygen gases in water electrolysis and modeling of the nucleation rate is crucial to the development of population balance modeling.

As illustrated in the previous nucleation experiments, expressing the surface concentration in terms of applied current is limited to ultra micro electrodes. Equation 3.9 can better relate the rate of nucleation for an electrolyzer provided the overpotential value.

#### 3.2 Bubble Growth

Growth is size enlargement of particles, by incorporation of single molecules from the continuous phase. It is given by the rate of increase of particle size. Growth involves a series of steps of the transport of solute molecules from the bulk liquid to the interface of the particle (mass transfer) and incorporation of the molecules in the particle structure (surface reaction / surface integration).

Table 3.1: Comparison of Nucleation Rate Measurements for  $\mathsf{O}_2$  and  $\mathsf{H}_2$  Nanobubbles

Aspect	O <sub>2</sub> Nanobubbles (Moreno Soto et al.)	H <sub>2</sub> Nanobubbles (German et al.)
Electrochemical Reaction	Oxidation: $H_2O_2 \rightarrow O_2 + 2H^+ + 2e^-$	Reduction: $2H^+ + 2e^- \rightarrow H_2$
Solution	$1~M~H_2O_2+1~M~HCIO_4$	$H_2SO_4$ (sulfuric acid)
Electrode Size	Pt nanoelectrodes, radii 3–51 nm	Pt nanoelectrodes, radii 7–41 nm
Control Method	Galvanostatic (constant current) below $i_{ m pb}^0$	Galvanostatic (constant current) below peak current $(i_{ m p})$
Detection	Voltage spike due to electrode blockage	Voltage spike due to impeded $H^+$ transport
Surface Conditioning	Extensive ( $\sim \! 100$ cycles, e.g., 0.64 V dissolution, 0.89 V stabilization)	Initial voltammogram, no detailed conditioning
Measurement Protocol	${\sim}10$ measurements per $i_{\rm app},$ recondition after; 30-s timeout	320 total (40 per $i_{\rm app}$ , 8 currents) across multiple electrodes
Induction Time $(t_{\sf ind})$	7 ms–15 s (e.g., 11.3–12.0 nA, 41-nm electrode); 2–3 orders variability at $\sim 0.9i_{\rm pb}^0$	0.17–8.1 s at -30 nA, 3.3–8.4 ms at -33 nA (41-nm electrode); wide variability
Supersaturation	$\zeta = 1601050 \text{ (very high)}$	$C_{\mathrm{H}_2}^{\mathrm{surf}} = 0.21$ –0.26 M (moderate, near critical 0.23 $\pm$ 0.02 M)
Nucleus Radius	${\sim}10$ nm (radius of curvature)	4.4–5.3 nm (41-nm electrode); 4.3–7.3 nm (all electrodes)
Contact Angle $(\theta)$	$135155^\circ$ (heterogeneous)	$148158^{\circ}$ (heterogeneous, e.g., $150^{\circ}$ for 41-nm electrode)
Molecules in Nucleus	50–900 $O_2$ molecules	$35-55~{ m H}_2~{ m molecules}$ (41-nm electrode)
Activation Energy $(E_a)$	6–30 <i>kT</i>	14–26 $kT$ (41-nm electrode); 7–28 $kT$ (all electrodes)
Internal Pressure	$\sim$ 14.2 MPa ( $\sim$ 140 atm)	270–330 atm (41-nm electrode)

Release of heat from the surface of the particle to the bulk liquid (heat transfer) may occur in parallel with the previous steps.

The growth of bubbles occurs due to net mass transfer into the bubble, which occurs when internal pressure exceeds the partial pressure of gas in the solution. Three key physical processes determine whether a bubble grows: (1) the flux of gas at the electrode surface (e.g. $J_{H_2}$ ) (2) the transport of gas in the solution phase, and (3) the internal pressure within the bubble, resulting in molecular transfer from the solution to the gas phase [30].

The concentration of dissolved gas in the bulk differs from that at the electrode-electrolyte interface, influencing the net mass transfer into the bubble. At the interface, rapid hydrogen production drives swift bubble growth, while in the bulk, the concentration remains close to equilibrium, resulting in minimal growth. Consequently, the bubble growth on the surface and in the bulk are analyzed separately.

the sizes of some bubbles still grow after they have detached from the surface, suggesting that the bubbles might keep growing even after detaching from the cathode surface as long as the surrounding liquid remains supersaturated [direct copy insitu]

#### 3.2.1 Growth on the electrode surface

Hydrogen bubble growth on the electrode surface predominantly driven by the hydrogen evolution reaction (HER). Three possible modes of bubble growth have been identified: inertia-controlled growth, diffusion-controlled growth, and "direct injection" growth. Bubble growth can be generally described by an empirical equation,  $R(t)=At^{\beta}$  where R(t) is the bubble radius,  $\beta$  is the growth coefficient, and A is a proportionality constant.

- Inertia controlled growth occurs initially but lasts only a very short time (0.01 s) before transition to the diffusion-controlled mode. Bubble growth is governed by the momentum interaction between the bubbles and ambient fluid with a value of  $\beta = 1$ .
- Diffusion controlled where the growth is controlled by the diffusion of dissolved gas into the bubble and  $\beta=0.5$  is expected.
- Direct injection mode means that all of the gas species are directly injected into a bubble. The growth of the radius is  $R \approx t^{\frac{1}{3}}$ , or  $\beta = \frac{1}{3}$ . This growth mode has been observed for  $H_2$  and  $O_2$  bubbles on electrodes at high current densities [31].

Diffusion controlled mode of growth dominated when the spacing between the bubbles on the electrode is large while at closer proximity the direct injection mode prevails [43].

The change in the radius of bubble during growth on the electrode surface is given by Scriven model [44].

$$R = 2\beta\sqrt{Dt} \tag{3.30}$$

The growth coefficient  $\beta$  is the function of the supersaturation for diffusion controlled growth [45]. The driving force can be expressed as:

$$\phi = \frac{RT}{P}(C_b - C_s) \tag{3.31}$$

27

Chapter 3. Bubble Evolution in Alkaline Water Electrolysis

where  $C_b$  is the bulk concentration and  $C_s$  is the saturation concentration. It is also given by the following equation in terms of the growth coefficient.

$$\phi = \frac{2\beta^2}{1 + 2\beta} \tag{3.32}$$

The dynamic growth rate can be evaluated by considering the mass balance on the surface concentration of hydrogen gas.

#### 3.2.2 Bubble growth in the bulk electrolyte

Once bubbles detach from the electrodes, their growth in the bulk electrolyte is generally slower and primarily diffusion -controlled. For diffusion-controlled growth in supersaturated solution, the rate of bubble growth can be expressed as

$$\frac{dR}{dt} = \frac{D(C_{\infty} - C_0)}{\rho_G} \left(\frac{1}{R} + \frac{1}{\sqrt{\pi Dt}}\right) \tag{3.33}$$

where  $D\ (m^2\ s^{-1})$  is the mass diffusivity coefficient of gas in the electrolyte [46].

In the bulk, the concentration of the dissolved gas  $C_{\infty}$  is approximately equal to the saturation concentration [47]. This leads to a low supersaturation in the bulk electrolyte and the growth rate is minimal.

At longer times the above equation rearranges to  $R\approx t^{\frac{1}{2}}$  which describes the second stage of growth on the surface of the electrode. However, the supersaturation should be the local value at the electrode-electrolyte interface.

#### 3.2.3 Levels of Concentration

To appropriately express the change in concentration at the electrode and in the bulk, the mass transfer around the electrode needs to be considered.

In electrochemical reactions at the electrode surface not all the gas produced converted to the gas phase, bubble. The following diagram represents the fluxes associated with it.

The amount of gas produced at the electrode,  $N_D$ , is given by

$$N_D = N_E + N_G$$

where  $N_E$  flux density to the bulk of the liquid, and  $N_G$  flux density to bubbles adhering to the bubble.

The amount of gas produced at the electrode is given by:

$$N_D = \frac{i}{zF}$$

and the flux density to the bulk of the liquid

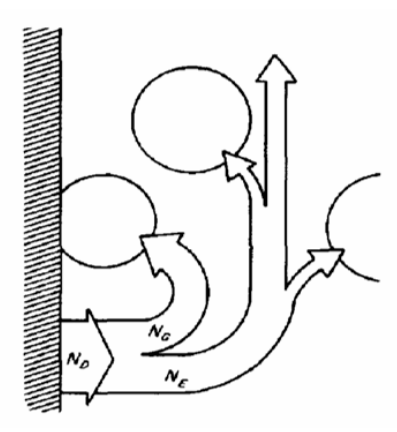


Figure 3.2: Transport mechanism of dissolved gas from the electrode [48].

$$N_E = k(C_{surf} - C_{\infty})$$

where k is the mass transfer coefficient. The fraction of evolved gas in form of bubbles grown at the electrode surface written as,  $f_G$ ,

$$f_G = \frac{N_G}{N_D} = 1 - \frac{N_E}{N_D}$$

It is given as a function of bubble coverage as [49]:

$$f_G = 1 - (1 - \Theta)^{2.5} \tag{3.34}$$

Two competing mechanisms result in the transport of hydrogen from the surface of the electrode. These are

- Convective mass transfer of dissolved substance from the electrode surface to the bulk of electrolyte and
- Primary transfer of dissolved substance from the region near the electrode to the gas-liquid interface of growing bubble adhering to the electrode, subsequent transformation into the gaseous phase and bubble departure from the electrode.

Different levels of concentrations exist in the system:

- The concentration at the surface of the electrode,  $C_{surf}$ , or  $C_e$ ;
- At the gas-liquid interface,  $C_0$   $C_i$
- Bulk concentration,  $C_{\infty}$ ,  $C_b$
- ullet Saturation concentration at equilibrium,  $C_{eqm}C_s$

Chapter 3. Bubble Evolution in Alkaline Water Electrolysis

The bulk concentration at gas-evolving electrodes roughly equals the saturation concentration, and the concentration at the gas-liquid interface roughly matches the concentration at the electrode before growth [47]. The supersaturation at the bubble-liquid interface may be estimated from the mass transfer equation of dissolved gas transported to liquid bulk,

$$\Delta C \approx C_{surf} - C_{\infty} \equiv \frac{N_E}{Ak} = \frac{I \varepsilon \nu}{AnFk} (1 - f_G)$$

Where  $N_E$  the flux of hydrogen gas transported to the bulk as given above, A the electrode surface area, k mass transfer coefficient,  $\varepsilon$  current efficiency,  $\nu$  is the stoichiometric number, and  $f_G$  is the gas evolution efficiency [47].

#### 3.3 Bubble Coalescence

Coalescence is the process by which two nearby bubbles merge to produce a single bubble. Since coalescence decreases the overall gas-liquid and gas-solid interfacial area, it is an energetically favorable process. The resulting geometry, the surfaces involved, and the pressures in the initial and final bubbles all affect the exact energy balance. The process entails the two bubbles combining in a non-equilibrium dumbbell shape, the drainage of the thin liquid film separating them, and a return to a more energetically advantageous (quasi spherical/sphere-cap) geometry.

Coalescence is dependent on the type of salts present in the electrolytic solution. Solution characteristics, including electrolyte, liquid phase rheology, and organic additives like surfactants and non-surface-active ethylene glycol, all affect the electrical characteristics of the gas-water interface and affect the behavior and coalescence of evolved bubbles during and after detaching from a solid surface [30]. At lower current densities, the coalescence of bubbles can be assumed negligible [21], [50]. This assumption taken into account in this work.

#### 3.4 Detachment

Detachment is the process of creating a free bubble that contains part or all of its constituent gas from an interfacial bubble. The process is governed by convective and interfacial forces, which can affect a bubble in an attractive or repulsive way. The increased energy of the liquid-gas interface compared to that of the solid-gas interface (which is small in hydrophilic and wetting surfaces) and fluid flow caused by local gradients in temperature and solute concentration results in an adhesive force. The forces that lead to bubble detachment are buoyancy, forced convection of the electrolyte, and coalescence between neighboring gas bubbles [30].

When the buoyancy force is greater than the interfacial tension between the electrode surface and the bubble, the bubbles detach from the electrode surface and start to rise uniformly [51]. The departure size of bubbles can be obtained from Fritz correlation [52] as:

$$x_d = 2 \times 0.0104 \ \theta \left[ \frac{\gamma}{g(\rho_L - \rho_G)} \right]^{0.5}$$
 (3.35)

Where  $\theta$  is the contact angle in degrees and it is found to be  $150^{\circ}$  for hydrogen in platinum nanoelectrodes [40],  $\gamma = 0.072~N/m$  is the surface tension of water, g gravitational acceleration, and  $\rho_L$  and

 $\rho_G$  the density of water  $997~kg/m^3$  and density of hydrogen gas  $0.089~kg/m^3$  respectively. Using these parameters the departure diameter becomes 8.22~mm.

However, compared to experimental findings in alkaline water electrolysis, this computed departure diameter (8.22 mm) is noticeably greater. A departure diameter of  $58~\mu m$  in the electrolysis of NaOH using stainless steel electrodes reported in the work of Cho et al. (2021) [51]. According to Liu et al. (2024) a hydrogen bubble departure diameter of less than  $60~\mu m$  found using nickel wire electrodes under industrial conditions (current densities  $0.15-0.35~A/cm^2$ ).

The discrepancy between the Fritz formula and experimental values may attributed to the full bubble behavior not captured by the Fritz formula which is mainly force balance. The departure diameter is dependent on the electrode material, surface properties, superficial velocity, temperature, concentration, and current density.

The rate at which the bubbles detach from the electrode surface can be viewed as the frequency of detachment. Once the residence time of hydrogen bubbles on the electrode surface determined, the frequency value can be taken as the inverse of the residence time of bubbles from experimental observations. A residence time of 0.012~s, recorded for hydrogen bubbles at a current density of  $100~mA/cm^2$ , with an electrolyte flow velocity of 13.3~cm/s in the work of Zhang et al. 2016 [50] which gives a frequency of  $83.3~s^{-1}$ . In another work by Cho et al (2021) [51] the residence time of bubbles from growth to detachment from the electrode surface was 533~ms, with a corresponding frequency of  $1.876~s^{-1}$ , rounded to  $2~s^{-1}$  used in the population balance modeling.

# 3.5 Additional Points regarding to the bubble behavior of Oxygen and Hydrogen

Hydrogen and oxygen bubbles exhibit distinct behaviors during electrolysis, as noted in [53], and [50]:

- Oxygen bubbles nucleate less frequently and tend to coalesce more readily than hydrogen bubbles.
- Hydrogen bubbles are typically smaller in size compared to oxygen bubbles.

This difference is due to stoichiometry because the volume of oxygen gas is half that of hydrogen, and oxygen bubbles adhere more tightly to the electrode. Furthermore, there is an electrical repulsion force between the negative cathode and the hydrogen bubbles that are also negative in water, causing the hydrogen bubbles to detach more easily at a smaller size [50].

#### 3.6 Conclusion

Based on the previous discussions the following key points drawn:

- Bubble Growth and supersaturation: Due to varying supersaturation levels at the electrodeelectrolyte interface and in the bulk, bubble growth dynamics differ and must be modeled separately.
- **System Boundaries**: Analysis of the bulk electrolyte and the electrode-electrolyte interface must be done separately due to their different boundaries.

- **Nucleation**: Nucleation process is unique to the electrode surface which justifies separate studies.
- **Population Balance Model**: Independent population balance models should be developed for the electrode surface and bulk electrolyte to capture the bubble evolutions in these systems.
- Particle Distribution for Simulation: The number distribution of bubbles departing from the electrode surface can serve as an input for bulk electrolyte simulations, applicable in both Euler-Euler and Euler-Lagrange frameworks.

# Chapter 4

# Population Balance Model Development

#### 4.1 Model Description

The modeling strategy chosen depends on the specific system selected. The electrolyte- electrode interface in alkaline water electrolysis is the system used in this project. Specifically, hydrogen bubble population balance modeling in the cathode compartment.

The first step in developing a population balance model is selecting an appropriate internal coordinate that characterizes the dispersed phase of the system [11]. For the present model, the bubble size, expressed in terms of diameter, is chosen as the internal coordinate. This allows the model to track the evolution of the hydrogen bubble size distribution over time due to nucleation, growth, and detachment processes.

The population balance equation (PBE) that describes the behavior of hydrogen bubbles can be written as:

$$\frac{\partial n(x,t)}{\partial t} + \frac{\partial (G(x,t)n(x,t))}{\partial x} - \frac{\partial}{\partial x} \left( D_x \frac{\partial n(x,t)}{\partial x} \right) = J(x,t) - D(x,t)$$
 (4.1)

• **Growth rate**: The growth rate describes the rate of change in the size of bubbles. Rearranging Equation 3.30 for x, the growth rate is given by [21]. Where  $\beta$  is the growth coefficient and equals 0.15, and D is the diffusivity of the hydrogen gas.

$$G(x) = \frac{8\beta^2 D}{x} \tag{4.2}$$

• Diffusivity in the Phase Space:

In alkaline water electrolysis, bubble growth rates vary significantly due to fluctuations in local supersaturation and electrode surface properties. This leads to the dispersion which must be

accounted for in the modeling. To capture this behavior, the diffusivity in the phase space,  $D_x$ , introduced following the approaches outlined by Marchisio et al.(2005) [54] and Askari et al. (2018) [15].

The value of  $D_x = 1 \times 10^{-10} m^2/s$  is derived from the molecular diffusivity of hydrogen gas to satisfy the Courant-Fredrichs-Lewy (CFL) condition, ensuring numerical stability in the solution of the population balance equation.

• **Detachment term**: This loss term indicates the removal of bubbles from the interface. Bubbles detach from the electrode surface when the size reaches the departure size. The rate of departure of bubbles can be expressed by the departure frequency, how frequent the bubbles leave the surface multiplied by the number density function, With these, the loss term is given by:

$$D(x,t) = f(x) n(x,t)$$
(4.3)

When bubble sizes are smaller than the departure size, the departure term, f(x), has a value of zero; when they are larger, the frequency, f, is present.

$$f(x) = \begin{cases} 0 & x < x_d \\ f & x \ge x_d \end{cases} \tag{4.4}$$

The departure size,  $x_d = 60 \ \mu m$ , and frequency of  $2 \ s^{-1}$  is used for the model.

Nucleation rate: The nucleation of bubbles is the source term in the above population balance
equation. Its rate is determined from the classical nucleation theory in the following subsection. Nucleation occurs at the critical size, minimum size of bubbles, and used as a boundary
condition.

Initial and boundary conditions:

$$n(x,0) = 0 \tag{4.5}$$

$$n(x_{min}, t) = \frac{J}{G(x_{min})} \tag{4.6}$$

#### 4.1.1 Nucleation rate

The calculation of the nucleation rate follows from the discussion of section 3.1. Recalling Equation 3.1:

$$J = J_0 \exp\left(\frac{-16\pi\gamma^3\phi(\theta)}{3k_BT \left(P_{gas} - P_0\right)^2}\right)$$
(4.7)

The parameters used to calculate the nucleation rate are presented in the following table. The nucleation rate becomes  $5.43 \times 10^{13} \ nuclei/m^2 s$  using the values in the table. Since the minimum size of bubbles that a camera may detect is determined by its resolution, this huge number of bubbles has not been reported in experimental works. For example, bubbles of size below  $60\mu m$  were not detected from R. Lira Garcia Barros et al. (2025) [9] .

Parameter	Value	Remark
Pre exponential factor, $J_0$ ,	$10^{20} nuclei/m^2s$	[40]
Contact angle, $ heta$	150°	[40]
Surface tension, $\gamma$	$0.072 \ N/m$	
Critical Radius, $R_c$	1.5 nm	[34]
Temperature, $T$ ,	298~K	Room temperature
Pressure, $P_0$	$101.325 \ kPa$	Atmospheric pressure
Henry's constant $H_2$ ,	$7.8 \times 10^{-6} mol \ m^{-3} Pa^{-1}$	[55]
Critical concentration, $C_{bn}$	$278.52 \ mol \ m^{-3}$	3.4
Bubble pressure, $P_{gas}$	35.7 MPa	Henry's law

Table 4.1: Parameters used for the nucleation rate.

#### 4.1.2 Solution to the PBM

The upwind implicit discretization scheme [22] is used to solve the population balance equation as follows:

$$\frac{n_i^{k+1} - n_i^k}{\Delta t} + \frac{G_i n_i^{k+1} - G_{i-1} n_{i-1}^{k+1}}{\Delta x} - D_x \frac{n_{i+1}^{k+1} - 2n_i^{k+1} + n_{i-1}^{k+1}}{\Delta x^2} = -f_i n_i^{k+1}. \tag{4.8}$$

$$-Fo \, n_{i+1}^{k+1} + \left[1 + \frac{\Delta t}{\Delta x} G_i + \Delta t \, f_i + 2Fo\right] n_i^{k+1} - \left[\frac{\Delta t}{\Delta x} G_{i-1} + Fo\right] n_{i-1}^{k+1} = n_i^k \tag{4.9}$$

where  $Fo = \frac{\Delta t}{\Delta x^2} D_x$ .

The boundary condition, BC at i=0:

$$n_0^{k+1} = \frac{J}{G(x_0)} \tag{4.10}$$

If the boundary condition is only imposed at the initial time step, which is one-time nucleation, the PBE depicts the number density evolution of nucleating bubbles without continuous addition of the nucleating bubbles. In this sense, both one-time and ongoing nucleation are discussed.

$$\left[1 + \frac{\Delta t}{\Delta x}G_i + \Delta t f_i + 2Fo\right] n_1^{k+1} = n_i^k + \left[\frac{\Delta t}{\Delta x}G_0 + Fo\right] \frac{J}{G(x_0)} + Fo n_2^{k+1} \tag{4.11}$$

The population balance equation solved for the size distribution and evolution of the mean diameters. The variation of three mean diameters  $d_{10}$ ,  $d_{32}$ , and  $d_{43}$  calculated from the moments of the distribution as:

$$d_{10} = \frac{m_1}{m_0}, \ d_{32} = \frac{m_3}{m_4}, \ d_{43} = \frac{m_4}{m_3}$$
 (4.12)

The size density of bubbles can also be calculated as:

$$f_{ni} = \frac{1}{x_{i+1} - x_i} \frac{N_i}{N_{tot}} \tag{4.13}$$

35

Chapter 4. Population Balance Model Development

Where  $N_i$  the total number of bubbles in the  $i^{th}$  class, and  $N_{tot}$  is the total number of bubbles at a time step. The total area under this curve was also calculated as a self-sanity check.

To demonstrate the applicability of the diffusivity element, the population balance model was first solved without it before introducing it.

# 4.2 Population Balance Modeling of Bubbles in $CO_2$ Supersaturated Water Solution

Taking into account, the similarity of nucleation mechanism, and availability of experimental data and discrete bubble modeling from the work of Battistella et al. (2021) [28], the same approach used to model the bubble size distribution of nucleating bubbles in super saturated  $CO_2$  solution. Here the growth rate is given by:

$$\frac{dx}{dt} = 2D\beta \left(\frac{2}{x} + \frac{1}{\sqrt{\pi Dt}}\right) \tag{4.14}$$

where  $\beta=(C_0-C_s)\rho_l/\rho_g MW$ ,  $D=1.97\times 10^{-9}m^2s^{-1}$ , the diffusion coefficient of  $CO_2$  in water,  $\rho_l=1000~kgm^{-3}$  is the liquid density,  $\rho_g=10.191~kg~mol^{-1}$  is the gas density at saturation pressure  $(P_s)$  and  $MW=44.01\times 10^{-3}kg~mol^{-1}$  is the molecular weight of  $CO_2$ .  $C_0$  and  $C_s$  are the bulk and saturation concentrations calculated from the Henry's constant  $(k_H=3.79\times 10^{-7}mol~kg^{-1}Pa^{-1}$  and the pressure before the run and after drop  $P_0$  and  $P_s$  [28].

The departure condition set by evaluating the Fritz radius using the mean values of the nucleation sites.

$$R_f = \left(\frac{3}{2} \frac{\gamma R_{site}}{(\rho_l - \rho_g)g}\right)^{\frac{1}{3}} \tag{4.15}$$

The value of  $R_{site}=40~\mu m$  the pore size of the surface taken from the work Battistella A. et al.(2021) [28] which gives the Fritz radius of  $7.14\times 10^{-4}m$  equals to  $x_d=1.43~mm$ . The corresponding departure frequency estimated to be  $f=0.1~s^{-1}$  by comparing the molecular weight of  $CO_2$  with  $H_2$ .

The critical bubble radius using the super saturation value,  $\zeta$  at a supersaturation value of  $\zeta=0.16$  is given by:

$$R_c = \frac{2\sigma}{p_s \zeta} \tag{4.16}$$

At  $\zeta = 0.16$  and  $P_s = 5.5 \ Bar, \ R_c = 1.34 \ \mu m.$ 

#### 4.2.1 Constant Supersaturation

For the first case constant supersaturation was assumed, and the bubble size distribution for nucleation and growth solved. Using the following rate equation, as an example, the population balance equation solved using  $D_x = 1 \times 10^{-12} \ m^2/s$ .

$$J = J_0 \exp\left(-\frac{k}{(\ln\zeta)^2}\right) \tag{4.17}$$

with  $J_0=1\times 10^{10}$ , and k=5, and  $\zeta$  is the supersaturation.

#### 4.2.2 Variable Supersaturation

In this scenario, the population balance equation is coupled with the species balance equation. The change in bulk concentration of  $CO_2$  and its supersaturation value in the system obtained from the mass balance on  $CO_2$ .

Mass transfer into a single bubble where  $k_L$  is the mass transfer coefficient a function of the bubble diameter, x, C and  $C_s$  is the bulk and saturation concentration:

$$m = k_L(x) \cdot A_b(x)(C - C_s) \tag{4.18}$$

From Sherwood number:

$$k_L = \frac{Sh \cdot D}{r} \tag{4.19}$$

Where D is the diffusion coefficient of  $CO_2$ . Area of a single bubble assuming a full sphere:

$$A_b = \pi x^2 \tag{4.20}$$

Substituting these values:

$$m = k_L(x) \cdot A_b(x)(C - C_s) = \pi \cdot Sh \cdot x \cdot D(C - C_s)$$
(4.21)

The number of bubbles in the size range (x, x + dx) is n(x, t) dx. The total number of bubbles is obtaining by integrating for the whole size range. The total amount of mass consumed by the growing bubbles per unit of volume given as:

$$m_{tot} = \int_0^\infty m(x)n(x,t) dx = \int_0^\infty \pi \cdot Sh \cdot x \cdot D(C - C_s)n(x,t) dx$$
 (4.22)

For diffusion controlled bubble growth Sh = 2:

$$m_{tot} = 2\pi D(C - C_s) \int_0^\infty x n(x, t) dx$$
(4.23)

The integral is evaluated as:

$$\int_0^\infty x n(x,t) = N_{tot} \cdot m_1 \tag{4.24}$$

Where  $N_{tot}$  is the total number of bubbles, and  $m_1$  is the first moment of the number density function. n(x,t) which represents the mean bubble size.

$$m_1 = \frac{\int_0^\infty x n(x,t)}{\int_0^\infty n(x,t)} = \frac{\int_0^\infty x n(x,t)}{N_{tot}}$$
(4.25)

37

Chapter 4. Population Balance Model Development

Thus,

$$m_{tot} = 2\pi D(C - C_s)N_{tot}m_1 \tag{4.26}$$

The nucleating vessel described in the work of Battistella A. (2021) [28] is a closed system. The mass balance applied here is for such closed systems.

The mass balance included the spatial diffusion in the system and sink term, the consumption by the growing bubbles. For one dimensional diffusion, the following equation adapted the thesis work of of Hilde Sjoerdstra [56], by changing the sink term from individual bubble consumption to the consumption by the population of bubbles.

$$\frac{\partial C}{\partial t} = D \frac{\partial^2 C}{\partial L^2} - 2\pi D(C - C_s) N_{tot} m_1$$
(4.27)

Where L is the spatial variation. Under this consideration the population balance equation becomes bi variate and is written as:

$$\frac{\partial n(x;L,t)}{\partial t} + \frac{\partial (G(x,t)n(x;L,t))}{\partial x} - \frac{\partial}{\partial x} \left( D_x \frac{\partial n(x;L,t)}{\partial x} \right) = J(x;L,t) - D(x;L,t)$$
 (4.28)

Here, the bubble number density is a function of the spatial location, L, and the size of bubbles, x. This makes the population balance equation dependent on the position and size of bubbles. For simplicity, the spatial variation is neglected.

The simplified mass balance equation becomes:

$$\frac{\partial C}{\partial t} = -2\pi D(C - C_s) N_{tot} m_1 \tag{4.29}$$

The supersaturation now can be calculated through time as

$$\zeta = \frac{C(t) - C_s}{C_s} \tag{4.30}$$

The coupled population balance equation solved using an upward implicit discretization, as described in the previous section, by same initial and boundary condition. An initial pressure of  $P_O=8.0\ Bar$ , and a saturation of  $P_s=1\ Bar$  used in this case.

### Chapter 5

# **Results and Discussion**

#### 5.1 Hydrogen Bubble Size Distribution

The simulation results from the population balance modeling of hydrogen bubble formation are presented here. First, the case of one-time nucleation with the influence of phase space diffusion is examined, followed by the continuous nucleation scenario. Presenting the results in this sequence highlights the progression of model development and emphasizes the significance of each step in capturing the underlying physical processes.

#### 5.1.1 One - time Nucleation

The bubble size distribution for the one-time nucleation case is shown in Figure 5.1, comparing two modeling scenarios: one without and one with phase-space diffusion. In the case with diffusion (Figure 5.1a), the distribution exhibits sharp peaks with discrete changes over time. This represents a growth rate-dominated regime, where very high growth rates occur at smaller bubble sizes. However, these peaks lack the natural spread typically observed in experimental studies. As a result, the simulated distribution deviates significantly from the experimental bubble size distribution shown in Figure 5.2, which shows hydrogen bubbles on the surface of a stainless steel cathode from the work of Cho et al. (2021) [51].

In contrast, Figure 5.1b incorporates the diffusion term in size space, capturing the variability in individual bubble growth. This behavior can be directly compared with the experimental bubble size distributions in Figure 5.2. Although discrepancies remain in the predicted versus experimentally determined bubble sizes, the results demonstrate that accounting for additional bubble phenomena within the population balance framework leads to improved predictive capability.

In both cases, the number distribution gradually decreases once no new bubbles nucleate after the given time step. When bubbles begin to detach from the surface, marked by the detachment threshold, the number density drops sharply, accompanied by a relatively broader distribution due to the reduced growth rate.

Figure 5.3 illustrates the evolution of the number mean  $(d_{10})$ , surface mean  $(d_{32})$ , and volume mean  $(d_{43})$  diameters. At early stages, the lower x values result in a high growth rate. Over time, the

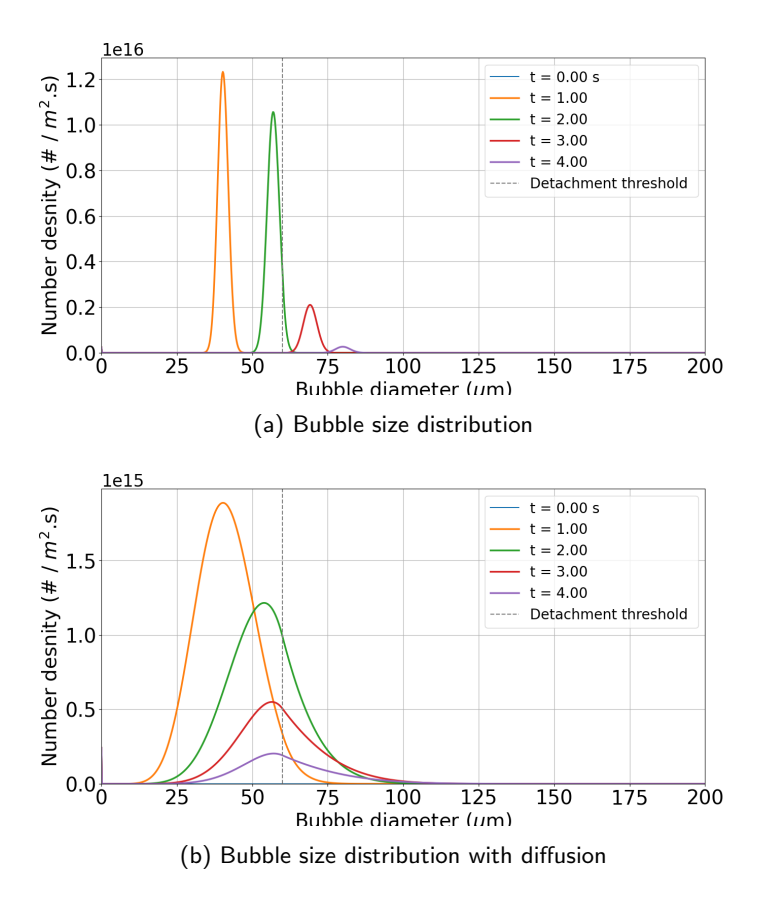


Figure 5.1: Comparison of bubble size distributions without and with diffusivity

growth rate declines, likely due to the detachment of larger bubbles. This trend is consistent across all three diameter measures. In the absence of phase-space diffusion, their values remain nearly identical, whereas the inclusion of phase-space diffusion introduces fluctuations, indicating a broader spread of bubble sizes.

#### 5.1.2 Continuous Nucleation

In this continuous nucleation scenario, new nuclei are introduced at every time step and the bubble size distribution is shown in Figure 5.4 (a). Initially, the bubble size distribution shifts to the right due to growth, but it eventually stabilizes as nucleation, growth, and detachment reach a dynamic balance. The sharp cutoff at approximately  $60~\mu m$  corresponds to the detachment threshold. The evolution of the mean diameters  $d_{10}$ ,  $d_{32}$ , and  $d_{43}$  in Figure 5.4 (b) shows a rapid initial increase, reflecting a faster growth rate, followed by a plateau as the effects of detachment dominate. The significant variation between the diameter values also an indication of the broader size distribution.

In this scenario, the bubble size distribution reaches a steady state that closely mirrors the experimental observations in Figure 5.2. The model accuracy could be further enhanced by incorporating the coalescence of smaller bubbles on the electrode surface, refining the departure condition, and cou-

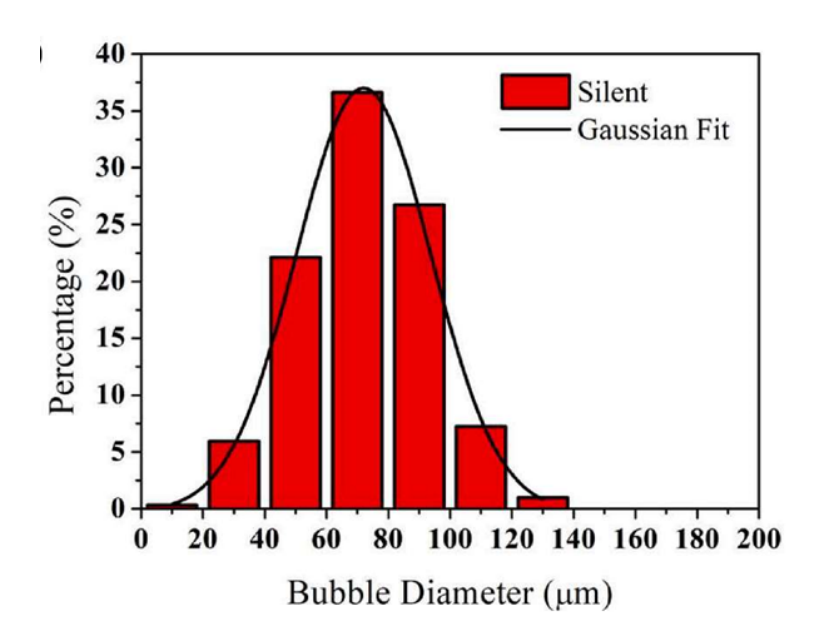


Figure 5.2: Experimental bubble size distribution [51]

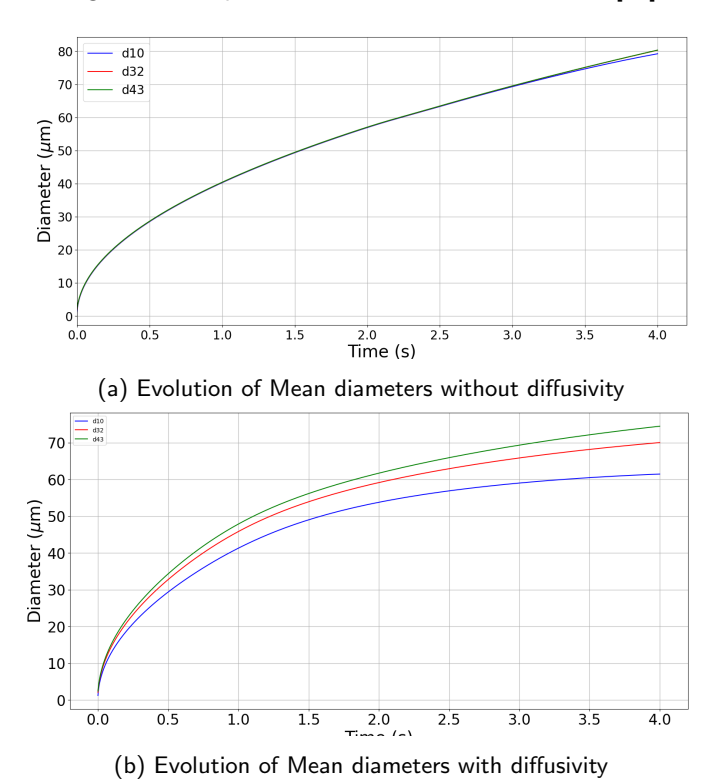


Figure 5.3: Comparison of mean diameters evolution without and with diffusivity

pling the mass balance with the population balance equation. Under the same modeling framework, experimental bubble size distributions would serve as valuable benchmarks for both validation and refining the model.

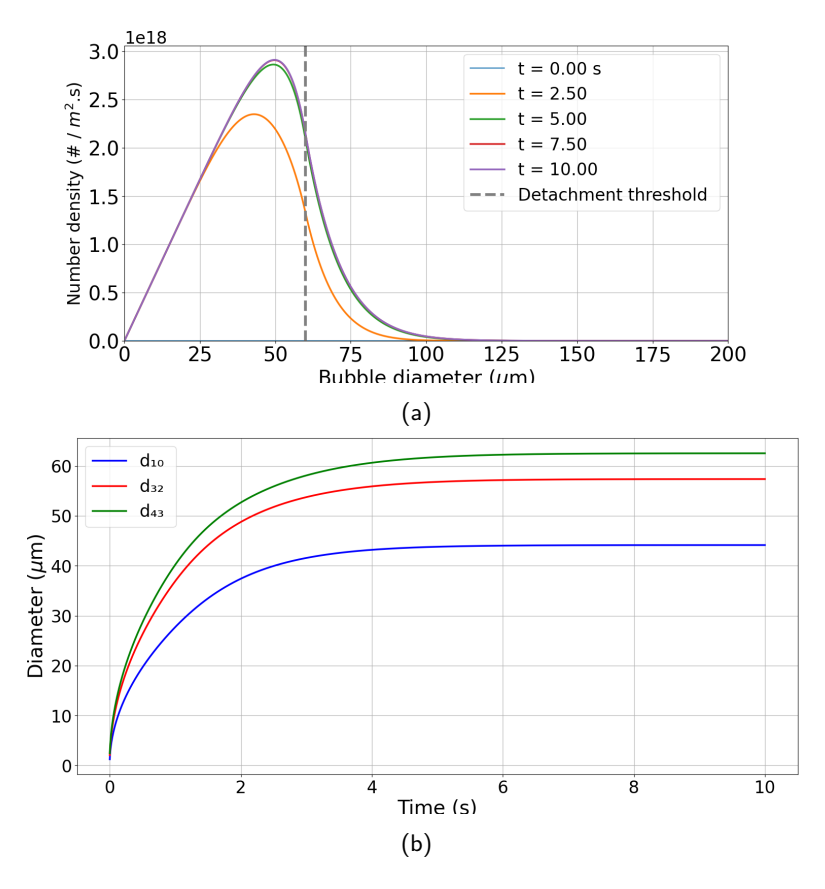


Figure 5.4: Bubble Size distribution (a) and Mean diameter evolution (b) under continuous nucleation

### 5.2 Bubble Size distribution in $CO_2$ supersaturated solution

The population balance modeling approach was applied to predict the size distribution of  $CO_2$  bubbles in supersaturated solutions. The model incorporates updated formulations for bubble growth and detachment criteria. Predictions are presented for both constant supersaturation and time-dependent supersaturation scenarios, enabling comparison of how the modified growth rate and detachment rule influence the evolving bubble population.

#### 5.2.1 Constant Supersaturation

At the beginning one time nucleation without and with phase space diffusion is applied at constant supersaturation of the  $CO_2$  solution. The initial and final pressure values are taken as  $P_o=6.4\ bar$  and  $P_s=5.5\ bar$  with a supersaturation of 1.16. The bubble size distribution at different time scales is shown in Figure 5.5. The result resembles the discrete distributions of the hydrogen bubbles. The

inclusion of the diffusivity in this case doesn't have an effect in the distribution. This is may be due to the growth rate dominate more than the variability of growth rate of  $CO_2$  bubbles. This can also indicate that the properties of the gas type and their growth rate form determines the modeling approach and the subsequent bubble size distributions.

#### 5.2.2 Variable Supersaturation

With a change in supersaturation, the bubble size distribution—illustrated in Figure 5.6—exhibits a relatively broader spread. This wider distribution may be attributed to the gradual decline in growth rate as supersaturation decreases over time. In both scenarios discussed above, the phase space diffusivity is evaluated under the assumption of one-time nucleation. Due to time constraints, the continuous nucleation analysis for both cases remains ongoing and is therefore not included in the current presentation.

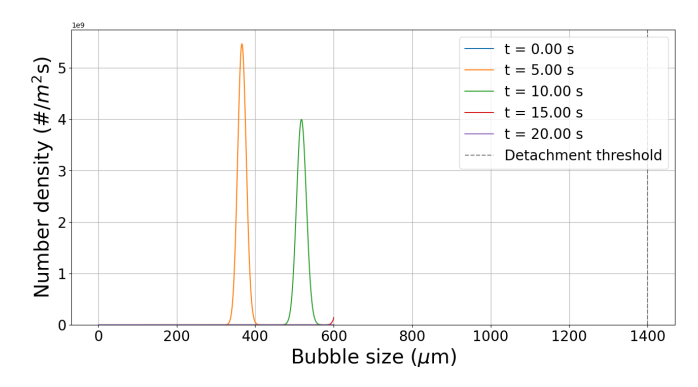


Figure 5.5: Bubble size distribution in  $CO_2$  bubbles

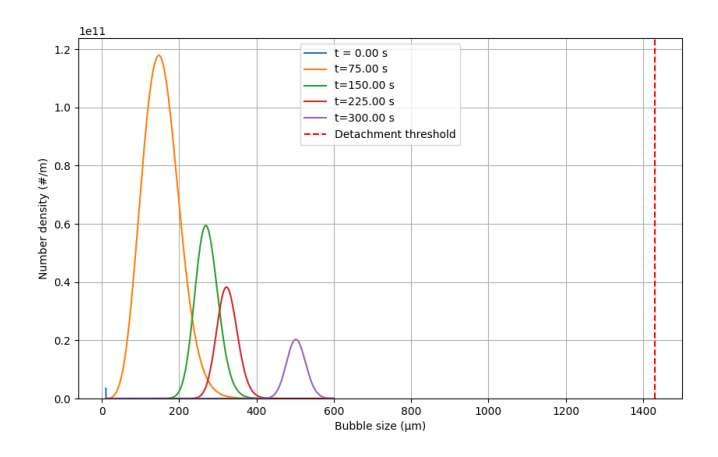


Figure 5.6: Bubble size distribution in  $CO_2$  bubbles with variable supersaturation

# Chapter 6

### **Conclusion and Outlook**

#### 6.1 Conclusion

In relation to the first research question, this project aimed to predict the bubble size distribution by population balance modeling within the cathode electrode-electrolyte subsystem in alkaline water electrolysis. To completely define the population balance equation, it was required to include equations describing bubble nucleation, growth, and detachment. While much of the existing literature concentrated on the behavior of individual bubbles, this work applied a structured approach to extend those insights to a broader population framework.

The nucleation of bubbles is the main source in modeling. Its rate is typically estimated via classical nucleation theory (CNT), which correlates the formation of critical nuclei to saturation levels at room temperature. This approach predicts the generation of a huge number of nanosized bubbles due to the high local gas supersaturation near the electrode. Although CNT provides a useful theoretical framework, its direct connection to electrochemical variables, such as current density, electrode morphology, and electrolyte characteristics, remains underexplored. Existing literature offers limited insight into these dependencies, suggesting a need for further investigation into the coupling between electrochemical parameters and nucleation dynamics.

Having the nucleation rate formulation, it can be easily integrated with the population balance equation. To facilitate the population balance modeling (PBM) within a multiphase simulation, it is essential to define the number and activity of nucleation sites. These can be assigned based on artificial nucleation sites distributions, porous electrode structures, or from the catalyst loading of an electrode which reflects the active site density on the electrode surface.

The growth rate of bubbles determined using Scriven's model with a constant growth rate coefficient,  $\beta$ , from earlier publications. By including the diffusion term in the phase space, the variation in the bubble growth rate is addressed. Mass balance of the dissolved hydrogen gas including its generation by the hydrogen evolution reaction, transport to the bulk, and consumption by the nucleating and growing bubbles can be used to determine a time-dependent growth coefficient.

Molecular diffusion to the bubble -liquid interface, liquid inertia and viscosity, and surface tension effects influence the the growth rate of bubbles. Integrating the hydrodynamics from computational fluid dynamics (CFD) simulations could allow these parameters to be evaluated more accurately. One

of the growth mechanisms is that coalescence of smaller bubbles on the surface. Neglecting this phenomena may lead to underestimation of larger bubble formation and result in a narrower bubble size distribution than what is observed experimentally.

The detachment diameter is set by taking into account the variation between the Fritz correlation and experimental observations. To complete the detachment condition, experimentally measured residence times were used to evaluate the detachment frequency. A uniform detachment frequency was applied across the entire bubble population; however, this assumption will not consider the variability in the detachment condition of individual bubbles. This constraint suggests that a more complex, separate modeling approach could enhance the accuracy and predictive capability of the detachment criteria.

The developed model was solved to predict the bubble size distribution and the evolution of mean bubble diameters. When compared with experimental observations, a significant discrepancy was identified between the simulated and measured results. This variation suggests that the full complexity of bubble behavior may not be fully captured by the population balance modeling (PBM) framework employed. However, the model offers a useful starting point for additional research. It provides an organized method for comprehending bubble dynamics which can be refined through experimental data, and CFD couplings.

# 6.2 How can population balance modeling be used in discrete bubble modeling?

Alkaline water electrolysis are two-phase systems where the dispessed phase undergo various stages. Modeling electrolytic bubble behavior in water electrolysis is essential for understanding system efficiency, mass transfer, and gas evolution dynamics. The two major modeling frameworks are population balance modeling (PBM) and Discrete bubble modeling (DBM).

PBM describes the evolution of the number density of bubbles interms of size or other internal coordinates using the population balance equation. While the DBM tracks the dynamics of individual bubbles in space and time. A distinction between the two modeling approaches summarized in the last section of Chapter 2.

For systems having a large number of bubbles and undergoing fluctuations in properties, it is computationally intensive to track a large number of bubbles; they can be grouped into a number of classes. The PBM can be applied within the class, which is similar to the parcel-type Euler Lagrangian simulation. The bubbles in the same class may undergo growth, coalescence, and breakage. In this way, statistical information such as the mean bubble diameter, total surface area, and volume of a class can be obtained. A combined approach of applying the DBM to the electrode surface and introducing the PBM in the bulk electrolyte can also be suggested.

#### 6.3 Outlook

The model development is still growing, new ideas were incorporated throughout the work. The corresponding results were not compared against experimental observations thoroughly. Although the following tasks were planned to complete the project, they could not be executed within the available timeframe. Instead, they have been outlined as recommendations for future improvements to enhance the current work.

- Nucleation rate equation applicable to a particular electrode structure;
- Performing mass balance on the dissolved hydrogen concentration and development of a coupled population balance equation;
- Investigating the relation between the reaction kinetics, electrochemical parameters, with the population balance equation;
- Thoroughly investigate how multiphase simulation can be combined with the population balance model starting form the electrode modeling;
- Using another solution method and made comparisons.

- [1] N L Panwar, S C Kaushik, and Surendra Kothari. "Role of renewable energy sources in environmental protection: A review". In: *Renewable and Sustainable Energy Reviews* 15.3 (2011), pp. 1513–1524. ISSN: 1364-0321. DOI: 10.1016/j.rser.2010.11.037. URL: http://dx.doi.org/10.1016/j.rser.2010.11.037.
- [2] Omar Ellabban, Haitham Abu-rub, and Frede Blaabjerg. "Renewable energy resources: Current status, future prospects and their enabling technology". In: Renewable and Sustainable Energy Reviews 39 (2014), pp. 748-764. ISSN: 1364-0321. DOI: 10.1016/j.rser.2014.07.113. URL: http://dx.doi.org/10.1016/j.rser.2014.07.113.
- [3] Chunlan Mao et al. "Review on research achievements of biogas from anaerobic digestion". In: Renewable and Sustainable Energy Reviews 45 (2015), pp. 540-555. ISSN: 1364-0321. DOI: 10.1016/j.rser.2015.02.032. URL: http://dx.doi.org/10.1016/j.rser.2015.02.032.
- [4] Camilia Daoudi and Tijani Bounahmidi. "Overview of Alkaline Water Electrolysis Modeling". In: International Journal of Hydrogen Energy 49 (Jan. 2024), pp. 646-667. ISSN: 03603199. DOI: 10.1016/j.ijhydene.2023.08.345. URL: https://linkinghub.elsevier.com/retrieve/pii/S036031992304541X (visited on 02/09/2024).
- [5] Song Hu et al. "A comprehensive review of alkaline water electrolysis mathematical modeling". In: Applied Energy 327 (Dec. 2022). ISSN: 03062619. DOI: 10.1016/j.apenergy.2022. 120099.
- [6] Martin David and Carlos Ocampo-Martinez. "Current Status of Water Electrolysis for Energy Storage". In: *Comprehensive Renewable Energy, Second Edition: Volume 1-9* 1-4 (Jan. 2022), pp. 533–552. DOI: 10.1016/B978-0-12-819727-1.00039-X.
- [7] Jaeseung Lee et al. "Modeling of Gas Evolution Processes in Porous Electrodes of Zero-Gap Alkaline Water Electrolysis Cells". In: Fuel 315 (May 2022), p. 123273. ISSN: 00162361. DOI: 10.1016/j.fuel.2022.123273. URL: https://linkinghub.elsevier.com/retrieve/pii/S0016236122001429 (visited on 02/28/2024).
- [8] Robert Phillips and Charles W. Dunnill. "Zero Gap Alkaline Electrolysis Cell Design for Renewable Energy Storage as Hydrogen Gas". In: RSC Advances 6.102 (2016), pp. 100643–100651. ISSN: 2046-2069. DOI: 10.1039/C6RA22242K. URL: http://xlink.rsc.org/?DOI=C6RA22242K (visited on 03/15/2024).
- [9] Rodrigo Lira Garcia Barros et al. "Impact of nickel electrode geometry on the electrochemical performance and bubble dynamics of a zero-gap alkaline electrolyzer". In: *Journal of Power Sources* 630 (Feb. 2025). ISSN: 03787753. DOI: 10.1016/j.jpowsour.2024.236116.
- [10] Amir Taqieddin, Michael R. Allshouse, and Akram N. Alshawabkeh. "Editors' Choice—Critical Review—Mathematical Formulations of Electrochemically Gas-Evolving Systems". In: *Journal*

- of The Electrochemical Society 165.13 (2018), E694–E711. ISSN: 0013-4651. DOI: 10.1149/2.0791813jes.
- [11] Doraiswami. Ramkrishna. *Population balances: theory and applications to particulate systems in engineering.* Academic Press, 2000, p. 355. ISBN: 0125769709.
- [12] Alexander Vikhansky and Andrew Splawski. "Adaptive multiply size group method for CFD-population balance modelling of polydisperse flows". In: *Canadian Journal of Chemical Engineering* 93.8 (Aug. 2015), pp. 1327–1334. ISSN: 1939019X. DOI: 10.1002/cjce.22201.
- [13] Sanjeev Kumar and D Ramkrishna. ON THE SOLUTION OF POPULATION BALANCE EQUA-TIONS BY DISCRETIZATION-I. A FIXED PIVOT TECHNIQUE. Tech. rep. 8. 1996, pp. 1311– 1332
- [14] Mohsen Shiea et al. "Downloaded from www.annualreviews Numerical Methods for the Solution of Population Balance Equations Coupled with Computational Fluid Dynamics". In: (2025), p. 12. DOI: 10.1146/annurev-chembioeng. URL: https://doi.org/10.1146/annurevchembioeng-.
- [15] Ehsan Askari, Pierre Proulx, and Alberto Passalacqua. "Modelling of bubbly flow using CFD-PBM solver in openfoam: Study of local population balance models and extended quadrature method of moments applications". In: *ChemEngineering* 2.1 (Mar. 2018), pp. 1–23. ISSN: 23057084. DOI: 10.3390/chemengineering2010008.
- [16] Alexander Vikhansky. COMBINED MULTIFLUID-POPULATION BALANCE METHOD FOR POLYDISPERSE MULTIPHASE FLOWS. Tech. rep.
- [17] Guang Hu et al. "A mini-review on population balance model for gas-liquid subcooled boiling flow in nuclear industry". In: *Annals of Nuclear Energy* 157 (July 2021). ISSN: 18732100. DOI: 10.1016/j.anucene.2021.108174.
- [18] Ganesan Subramanian and Doraiswami Ramkrishna. MATHEMATICAL BIOSCIENCES On the Solution of Statistical Models of Cell Populations. Tech. rep. 1971.
- [19] Sanjeev Kumart and D Ramkrishna. On the solution of population balance equations by discretization-III. Nucleation, growth and aggregation of particles\*. Tech. rep. 24. 1997, pp. 4659–4679.
- [20] V. R. Marshall M. J. Hounslow R. L. Ryall. A Discretized Population Balance for Nucleation, Growth, and Aggregation. Tech. rep. 1988.
- [21] A W Bryson and D L Hofman. A population balance approach to the study of bubble behaviour at gas-evolving electrodes. Tech. rep. 1989.
- [22] Pavan K. Inguva, Kaylee C. Schickel, and Richard D. Braatz. "Efficient numerical schemes for population balance models". In: *Computers and Chemical Engineering* 162 (June 2022). ISSN: 00981354. DOI: 10.1016/j.compchemeng.2022.107808.
- [23] Doraiswami Ramkrishna and Meenesh R. Singh. *Population balance modeling: Current status and future prospects.* 2014. DOI: 10.1146/annurev-chembioeng-060713-040241.
- [24] Pierre Van De Velde et al. *Hydrogen bubble sizes, induced flow and coalescence around 1 model wire electrodes. 2.* Tech. rep. URL: https://ssrn.com/abstract=4949996.
- [25] Shuiqing Zhan et al. "3D Numerical Simulations of Gas-Liquid Two-Phase Flows in Aluminum Electrolysis Cells with the Coupled Model of Computational Fluid Dynamics-Population Balance Model". In: *Industrial and Engineering Chemistry Research* 56.30 (Aug. 2017), pp. 8649–8662. ISSN: 15205045. DOI: 10.1021/acs.iecr.7b01765.
- Thomas Nierhaus et al. "Simulation of the Two-Phase Flow Hydrodynamics in an IRDE Reactor". In: *Journal of The Electrochemical Society* 156.9 (2009), P139. ISSN: 00134651. DOI: 10.1149/1.3155423.

- [27] Yuanping He et al. "Coupling Eulerian-Lagrangian method of air-particle two-phase flow with population balance equations to simulate the evolution of vehicle exhaust plume". In: *International Journal for Numerical Methods in Fluids* 88.3 (Sept. 2018), pp. 117–140. ISSN: 10970363. DOI: 10.1002/fld.4514.
- [28] A. Battistella. *Hydrodynamics, Mass Transfer and Phase Transition in Bubbly Flows*. Tech. rep. 2021. URL: www.tue.nl/taverne.
- [29] Xiao Ying Wong, Yuting Zhuo, and Yansong Shen. "Numerical Analysis of Hydrogen Bubble Behavior in a Zero-Gap Alkaline Water Electrolyzer Flow Channel". In: *Industrial and Engineering Chemistry Research* 60.33 (Aug. 2021), pp. 12429–12446. ISSN: 15205045. DOI: 10.1021/acs.iecr.1c02554.
- [30] Paul A. Kempler, Robert H. Coridan, and Long Luo. *Gas Evolution in Water Electrolysis*. Oct. 2024. DOI: 10.1021/acs.chemrev.4c00211.
- [31] Xu Zhao, Hang Ren, and Long Luo. "Gas Bubbles in Electrochemical Gas Evolution Reactions". In: *Langmuir* 35.16 (Apr. 2019), pp. 5392–5408. ISSN: 15205827. DOI: 10.1021/acs.langmuir.9b00119.
- [32] S. Karthika, T. K. Radhakrishnan, and P. Kalaichelvi. "A Review of Classical and Nonclassical Nucleation Theories". In: Crystal Growth and Design 16.11 (Nov. 2016), pp. 6663–6681. ISSN: 15287505. DOI: 10.1021/acs.cgd.6b00794.
- [33] Álvaro Moreno Soto et al. "The Nucleation Rate of Single O2 Nanobubbles at Pt Nanoelectrodes". In: *Langmuir* 34.25 (June 2018), pp. 7309–7318. ISSN: 15205827. DOI: 10.1021/acs.langmuir.8b01372.
- [34] Jaeseung Lee et al. "Modeling of gas evolution processes in porous electrodes of zero-gap alkaline water electrolysis cells". In: *Fuel* 315 (May 2022). ISSN: 00162361. DOI: 10.1016/j.fuel.2022.123273.
- [35] M. P. Anisimov. "Nucleation: Theory and experiment". In: Uspekhi Khimii 72.7 (2003), pp. 664–706. ISSN: 00421308. DOI: 10.1070/rc2003v072n07abeh000761.
- [36] Matheus T. de Groot and Paul Vermeulen. "Advanced characterization of alkaline water electrolysis through electrochemical impedance spectroscopy and polarization curves". In: Journal of Electroanalytical Chemistry 974 (Dec. 2024), p. 118709. ISSN: 15726657. DOI: 10.1016/j.jelechem.2024.118709. URL: https://linkinghub.elsevier.com/retrieve/pii/S1572665724006878.
- [37] Z. Abdin, C. J. Webb, and E. Mac A. Gray. "Modelling and simulation of an alkaline electrolyser cell". In: Energy 138 (2017), pp. 316–331. ISSN: 03605442. DOI: 10.1016/j.energy.2017.07.053.
- [38] Dohyung Jang, Hyun Seok Cho, and Sanggyu Kang. "Numerical modeling and analysis of the effect of pressure on the performance of an alkaline water electrolysis system". In: *Applied Energy* 287 (Apr. 2021). ISSN: 03062619. DOI: 10.1016/j.apenergy.2021.116554.
- [39] Ronald Rojas Hacha et al. "Measurement and analysis of H2 and O2 bubbles diameter produced by electroflotation processes in a modified Partridge-Smith cell". In: *Powder Technology* 342 (Jan. 2019), pp. 308–320. ISSN: 1873328X. DOI: 10.1016/j.powtec.2018.09.062.
- [40] Sean R. German et al. "Critical Nuclei Size, Rate, and Activation Energy of H2 Gas Nucleation". In: Journal of the American Chemical Society 140.11 (Mar. 2018), pp. 4047–4053. ISSN: 15205126. DOI: 10.1021/jacs.7b13457.
- [41] Jiancheng Lin et al. Understanding the nanoscale phenomena of nucleation and crystal growth in electrodeposition. Oct. 2024. DOI: 10.1039/d4nr02389g.
- [42] Steven Lubetkin and Mark Blackwell. The Nucleation of Bubbles in Supersaturated Solutions. Tech. rep. 1988.

- [43] F. J. Higuera. "A model of the growth of hydrogen bubbles in the electrolysis of water". In: *Journal of Fluid Mechanics* 927 (Nov. 2021). ISSN: 14697645. DOI: 10.1017/jfm.2021.778.
- [44] L E Scriven. ON THE DYNAMICS OF PHASE GROWTH. Tech. rep.
- [45] S F Jones, G M Evans, and K P Galvin. The cycle of bubble production from a gas cavity in a supersaturated solution. Tech. rep. 1999.
- [46] P. S. Epstein and M. S. Plesset. "On the stability of gas bubbles in liquid-gas solutions". In: *The Journal of Chemical Physics* 18.11 (1950), pp. 1505–1509. ISSN: 00219606. DOI: 10.1063/1. 1747520.
- [47] H. Vogt, Ö Aras, and R. J. Balzer. "The limits of the analogy between boiling and gas evolution at electrodes". In: *International Journal of Heat and Mass Transfer* 47.4 (2004), pp. 787–795. ISSN: 00179310. DOI: 10.1016/j.ijheatmasstransfer.2003.07.023.
- [48] H Vogt. THE RATE OF GAS EVOLUTION AT ELECTRODES-I. AN ESTIMATE OF THE EFFICIENCY OF GAS EVOLUTION FROM THE SUPERSATURATION OF ELECTROLYTE ADJACENT TO A GAS-EVOLVING ELECTRODE. Tech. rep.
- [49] H. Vogt. "On the gas-evolution efficiency of electrodes. II Numerical analysis". In: Electrochimica Acta 56.5 (Feb. 2011), pp. 2404–2410. ISSN: 00134686. DOI: 10.1016/j.electacta. 2010.11.004.
- [50] Yifan Li et al. "In-situ investigation and modeling of electrochemical reactions with simultaneous oxygen and hydrogen microbubble evolutions in water electrolysis". In: *International Journal of Hydrogen Energy* 44.52 (Oct. 2019), pp. 28283–28293. ISSN: 03603199. DOI: 10.1016/j.ijhydene.2019.09.044.
- [51] Kyung Min Cho, P. R. Deshmukh, and Weon Gyu Shin. "Hydrodynamic behavior of bubbles at gas-evolving electrode in ultrasonic field during water electrolysis". In: *Ultrasonics Sonochemistry* 80 (Dec. 2021). ISSN: 18732828. DOI: 10.1016/j.ultsonch.2021.105796.
- [52] Çayan Demirkır et al. "Life beyond Fritz: On the Detachment of Electrolytic Bubbles". In: Langmuir 40.39 (Oct. 2024), pp. 20474–20484. ISSN: 15205827. DOI: 10.1021/acs.langmuir. 4c01963.
- [53] L J 1 Janssen et al. BUBBLE BEHAVIOUR DURING OXYGEN AND HYDROGEN EVOLUTION AT TRANSPARENT ELECTRODES IN KOH SOLUTION. Tech. rep.
- [54] Daniele L. Marchisio and Rodney O. Fox. "Solution of population balance equations using the direct quadrature method of moments". In: *Journal of Aerosol Science* 36.1 (2005), pp. 43–73. ISSN: 00218502. DOI: 10.1016/j.jaerosci.2004.07.009.
- [55] J. C. Garcia-Navarro, M. Schulze, and K. A. Friedrich. "Measuring and modeling mass transport losses in proton exchange membrane water electrolyzers using electrochemical impedance spectroscopy". In: *Journal of Power Sources* 431 (Aug. 2019), pp. 189–204. ISSN: 03787753. DOI: 10.1016/j.jpowsour.2019.05.027.
- [56] Hilde Sjoerdstra. Meso-Scale Modelling and Experimental Validation of Supersaturation Induced Bubble Growth on a Substrate. Tech. rep.
- [57] A. J. Bard, L. R. Faulkner, and Henry S. White. *Electrochemical Methods*. Tech. rep. New York: John Wiley and Sons, 2001.

# Appendix A

# **Appendix Title**

#### A.1 Concentration as a function of current

The following discussion taken from the book Electrochemical Methods Fundamentals and Application [57].

Consider a redox reaction on the surface of the electrode

$$O + ne^- \Leftrightarrow R$$

The rate of the reaction can be obtained from Faraday's law. The total charge transferred according to the Faraday's law of electrolysis

 $Q(coulombs) = nF(Coulombs/mol\ electrolyzed) * N(mol\ electrolyzed)$ 

The current which is the rate at which the total charge collected,

$$i = \frac{dQ}{dt} = nF\frac{dN}{dt} \tag{A.1}$$

For electrode reactions which occur at the electrode/electrolyte interface, the rate depends on mass transfer to the electrode and various surface effects, in addition to the usual kinetic variables.

Reaction rate,  $\nu$ , for heterogeneous reactions usually given in units of mol/s per unit area of electrode surface, A:

$$Rate(mol\ s^{-1}\ cm^{-2}) = \nu = \frac{i}{nFA} = \frac{j}{nF}$$
 (A.2)

Reaction mechanisms at the electrode

For the reaction given above, the following reaction steps are involved:

- Mass transfer
- Electron transfer at the electrode surface

- Chemical reactions preceding or following the electron transfer
- Other surface reactions such as adsorption, desorption, or crystallization

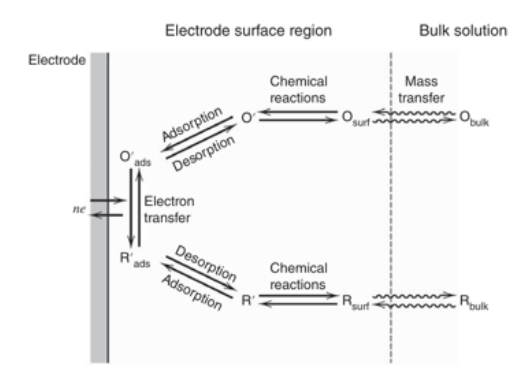


Figure 1.2.6 Pathway of a general electrode reaction.

Figure A.1: Pathway of a general electrode reaction [57]

Steady state current can be achieved when the rates of all reaction steps are the same. The rate determining step limits the magnitude of the current.

Fig reaction steps For a reversible electrode reactions, the net rate of the electrode reaction is governed totally by the rate at which the electro reactant is brought to the surface by mass transfer,  $\nu_{mt}$ 

$$\nu_{mt} = \pm \frac{i}{nFA}$$

(+ for a reduction, and - for an oxidation)

The rate of mass transfer to an electrode surface comprised of diffusion, migration of ions, and convective flow described by the Nersnt-Planck equation. For one dimensional mass transfer along  $\times$  axis

$$J_{i}(x) = -D_{j} \frac{\partial C_{j}(x)}{\partial x} - \frac{z_{j}F}{RT} D_{j}C_{j}(x) \frac{\partial \phi(x)}{\partial x} + C_{j}(x)v(x)$$
(A.3)

where

The flux of species j at the electrode surface,  $J_j(x=0)$  plays an important interpretation.

- Positive flux into the surface the rate at which species j is consumed by electrolysis
- Negative flux out of the surface the rate at which species j is produced by the electrode reaction.

Steady state mass transfer can be achieved in:

- Rotating disk electrode
- ullet Ultra micro electrodes (UME) of spheres, hemispheres, or disks of radii 10nm-25m

The flux at x=0

$$J_o(x=0) = -D_0 \left(\frac{dC_0}{dx}\right)_{x=0}$$

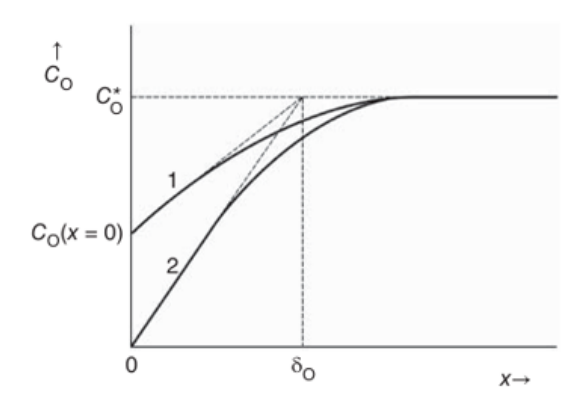


Figure A.2: Concentration profiles (solid lines) and diffusion-layer approximation (dashed lines). x=0 corresponds to the electrode surface, and  $\delta_O$  is the diffusion layer thickness [57]

Assuming a linear concentration gradient within the diffusion layer

$$J_0(x=0) = -D_0[C_0^* - C_0(x=0)]/\delta_0$$
(A.4)

The ratio  $D_0/\delta_0=m_0$  mass transfer coefficient

$$J_0(x=0) = -m_0[C_0^* - C_0(x=0)] \tag{A.5}$$

From the rate of the reaction and considering reduction occurring at the electrode,

$$\frac{i}{nFA} = m_0[C_0^* - C_0(x=0)] \tag{A.6}$$

At the same time, R is produced at the electrode surface, so that  $C_R(x=0)>C_R^*$ 

$$\frac{i}{nFA} = m_R[C_R(x=0) - C_R^*]$$
 (A.7)

Mass transfer coefficient value for the simple geometries

• Rotating electrode,

$$m_O = 0.62 D_O^{\frac{2}{3}} \omega^{\frac{1}{2}} v^{-\frac{1}{6}}$$

• Spherical UME of radius,  $r_O$ ,

$$m_o = D_0/r_0$$

 $\bullet$  Disk UME of radius,  $r_O$ ,

$$m_o = 4D_0/\pi r_0$$

For a Hydrogen evolution reaction/HER/ at the cathode,  $H_2$  is the reduced component. Substituting the mass transfer coefficient of the disk electrode:

Appendix A. Appendix Title

$$i = 4naFD_{H_2}(C_{H_2}^{surf} - C_{H_2}^{bulk})$$

where n is the number of electrons transferred per molecule generated  $H_2$  (n = 2), a is the radius of the disk electrode, F is the Faraday constant (96485 C / mol),  $D_{H_2}=4.5*10^5cm^2/s$  is the diffusion coefficient for  $H_2$  and  $C_{H_2}^{bulk}=0M$  is the concentration of  $H_2$  in the bulk solution.

Henry's law given by

$$C_{gas}^{surf} = P_{gas}K_H \tag{A.8}$$

Substituting the above equations, the rate of nucleation as a function of current is rearranged to

$$J = J_0 \exp\left(\frac{-16\pi\gamma^3\phi(\theta)}{3k_B T \left(\frac{i}{K_H 4n FaD_{H_2}} - P_{\text{ambient}}\right)^2}\right)$$
(A.9)

\*Disclaimer: Tools like ChatGPT and Grammarly have been used to check grammar mistakes, improve the academic style, and readability of the text".